Lawrence Berkeley Laboratory
UNIVERSITY OF CALIFORNIA

ENERGY & ENVIRONMENT DIVISION

COMBUSTION RESEARCH

Chapter from the Energy and Environment Division
Annual Report 1980

May 1981

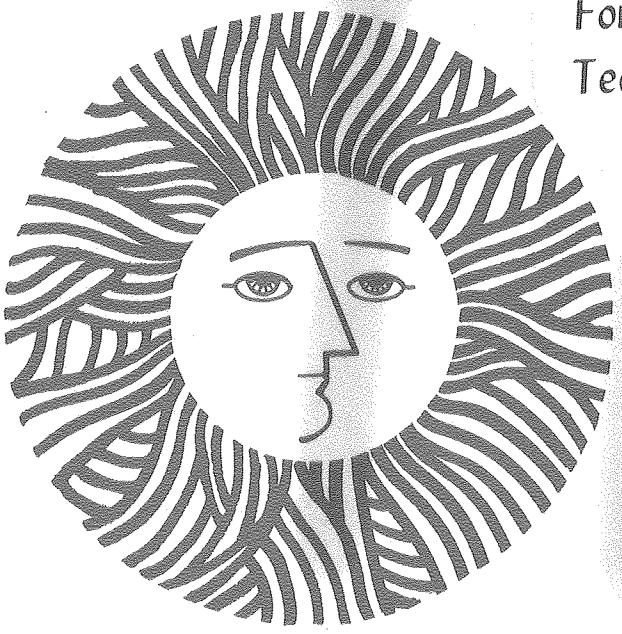

Prepared for the U.S. Department of Energy under Contract W-7405-ENG-48

DISCLAIMER

COMBUSTION RESEARCH
FY 1980

Lawrence Berkeley Laboratory
University of California
Berkeley, California 94720

Prepared for the U.S. Department of Defense under Contract No. W-7405-ENG-48.

CONTENTS

COMBUSTION RESEARCH PERSONNEL

FY 1980

A. W. Abdel-Hafez
M. J. Alpaugh
R. B. Bill
T. J. Brault
M. Q. Brewster
N. J. Brown
J. S. Brunetto
M. W. Chan
D. Y. Chen
R. K. Cheng
A. J. Chorin
A. Colpart
E. Cuellar
J. W. Daily
D. C. Edgin
F. L. Fisher
A. F. Ghoniem
C. E. Grant
R. Greif
E. Hahn
H. A. Heperkan
K. Hom
F. C. Hurlbut
B. A. Ingraham
C. M. Johnson
T. J. Kokoska
S. C. Ling
T. Liskam
D. Lucas
J. T. Metcalf
K. C. Metchette
M. A. Milan
M. Mohtasheni
J. Myomoto-Mills
M. Namazian
I. Namer
T. M. Ng
A. K. Oppenheim
R. C. Palmer
G. M. Parsons
J. Pennucci
R. B. Peterson
W. J. Pitz
O. M. I. Rashed
F. A. Robben
R. F. Sawyer
R. W. Schefer
P. M. Sherman
G. S. Shiralkar
G. Steere
H. E. Stewart
L. Talbot
C. L. Tien
P. J. Tierney
W. C. Tong
S. R. Vosen
R. B. Williamson
J. B. Woodard

INTRODUCTION

Combustion processes are an essential part of the utilization of more than 90% of the energy consumed in the United States, play important roles in the extraction and processing of fossil energy, are responsible for most of our air pollution, and are at the center of the field of fire safety. The art of combustion has been highly developed during the past hundred years, producing through trial and error a variety of combustion devices that convert chemical energy into thermal and mechanical energy. Traditional design methods can no longer meet the often competing demands of high efficiency, low pollutant emissions, and alternative fuels utilization. Combustion science is able to provide the fundamental understanding of combustion processes essential for the application of theory to the analysis and design of advanced combustion systems.

Combustion research at the Lawrence Berkeley Laboratory focuses on the study of the chemical and physical processes which are important in combustion. Two areas of application dominate; the control of combustion processes to allow the utilization of new fuels while limiting pollutant formation and the reduction of fire hazards accompanying energy generation and utilization technologies. Principal program areas are the interaction of fluid-mechanical turbulence and combustion, the development and application of new physical and chemical diagnostic techniques for combustion research, pollutant formation and destruction processes, theoretical and computational modeling of combustion processes, combustion processes in engines, fire science, and fire safety.

The research team consists of research scientists at the Lawrence Berkeley Laboratory, faculty and graduate students of the Departments of Mechanical and Civil Engineering at the University of California at Berkeley, visitors from throughout the United States and the world, and a supporting technical, clerical, and administrative staff.

A major component of the research program is the training of combustion scientists and engineers at all levels. The graduate program in combustion at the University of California at Berkeley is one of the largest and most diversified in the world. Laboratory facilities are located at the Lawrence Berkeley Laboratory, on the campus of the University of California, and at the Richmond Field Station. Cooperative research is conducted by Lawrence Berkeley Laboratory scientists with investigators at the Lawrence Livermore National Laboratory and at the Sandia National Laboratory Combustion Research Facility.

ENGINE COMBUSTION AND IGNITION STUDIES

MECHANISM OF INSTABILITIES IN TURBULENT COMBUSTION LEADING TO FLASHBACK*

J. Keller, L. Vaneveld, D. Korschelt,
G. Hubbard, A. Ghoniem, J. Daily, and A. Oppenheim

INTRODUCTION

In conventional combustors for gas turbines, the flame front is established at the stoichiometric contour in the primary zone.[1,2] This produces optimum conditions for the generation of pollutants. The best remedy for this state of affairs is offered by "lean, premixed/prevaporized combustors".[3,4] Such systems require the use of a premixing chamber while combustion is stabilized by a bluff body flame holder.[5] Their operation is handicapped by potentially harmful combustion instabilities.[6,7] At the lean limit, they cause blow-off; at the rich, they lead to flashback. The purpose of our studies is to explore the mechanism of the instabilities associated with the rich limit, under highly turbulent flow conditions.

ACCOMPLISHMENTS DURING FY 1980

The experiments were performed using our combustion tunnel depicted in Figure 1, p. 6-33, Energy and Environment Division Annual Report FY 1979. In this tunnel, the flame was stabilized by a streamlined contraction culminating in a rearward facing step. Propane/air mixtures were employed as the working substance, instabilities were triggered by a sudden increase in the flow rate of fuel, and observations were made using high speed schlieren cinematography combined with pressure measurements. As the rich limit was thus approached, we were able to identify three modes of instabilities called, for lack of better names, (1) humming, (2) buzzing, and (3) chucking.

In comparison to the flow field associated with stable combustion which was described in the 1979 Annual Report, the characteristic features of these instabilities are presented here in Figures 1, 2, and 3, all pertaining to the same inlet flow velocity of 13.3 m/sec as in Figure 1b of the 1979 Annual Report. The first was obtained when the pressure in the test section was maintained at a minimum level; the second, when it was slightly increased (about 10 mm of water) by closing a butterfly valve in the exhaust duct; the third was established when the equivalence ratio was at a flashback limit.

We attribute the mechanism of these instabilities to the interaction between the set of trailing vortices in the mixing region behind the edge of the step and the set of recirculation vortices formed behind its base. Salient features of this process are depicted schematically in Figure 4.

Shown in the sketch at the top of Figure 4 is the trailing vortex pattern associated with stable combustion. Here, the flame front delineates the outer edges of the mixing layer at the contour of the interface between the burned gases and the fresh charge. In the next photograph below, not detectable by schlieren optics, is the recirculation vortex, A, that is, as a rule, established behind the step irrespective of whether the flow field is associated with combustion or not. This gives rise to a counter-rotating vortex, B.

When more burned gases are produced in the presence of combustion, both of these vortices grow, as shown in the second sketch. The growing recirculation vortex of the burned gases causes vortex A to be pushed downstream, as shown in the third sketch, while vortex B increases in size. As a consequence of the counter clockwise circulation of this vortex, it must give rise to vortices C and D, as required by compatibility with the flow of the fresh charge. When vortex B becomes larger, as shown in the fourth sketch, vortex C may be forced upstream, causing a flow reversal on top of the step, tripping the boundary layer, and pushing the flame upstream. This, in our opinion, is the characteristic feature of turbulent flashback we observed. The flame front is attached at its upstream edge to the boundary layer; but, behind this edge, it is lifted from the wall by the action of vortex C.

As vortex B grows still further, it is convected downstream, while vortex C pairs with vortex D to form a new vortex A' and, concomitantly, a new corner vortex B', as shown in the fifth sketch. Finally vortex A' grows to a size comparable to that of Vortex A, and B' to B, as in the second sketch. At the same time, vortex B is convected further downstream and, as illustrated in the sixth sketch, the combined action of vortex A' and B causes the flame to acquire a practically vertical orientation, extending across the full height of the combustor.

* This work was supported by the Director of the Office of Energy Research, Office of Basic Energy Sciences, Engineering, Mathematics, and Geosciences Division of the U.S. Department of Energy under Contract No. W-7405-ENG-48 and by the U.S. National Aeronautics and Space Administration under Grant No. NSG 3227 through the Engineering Office of Research Services, University of California, Berkeley.

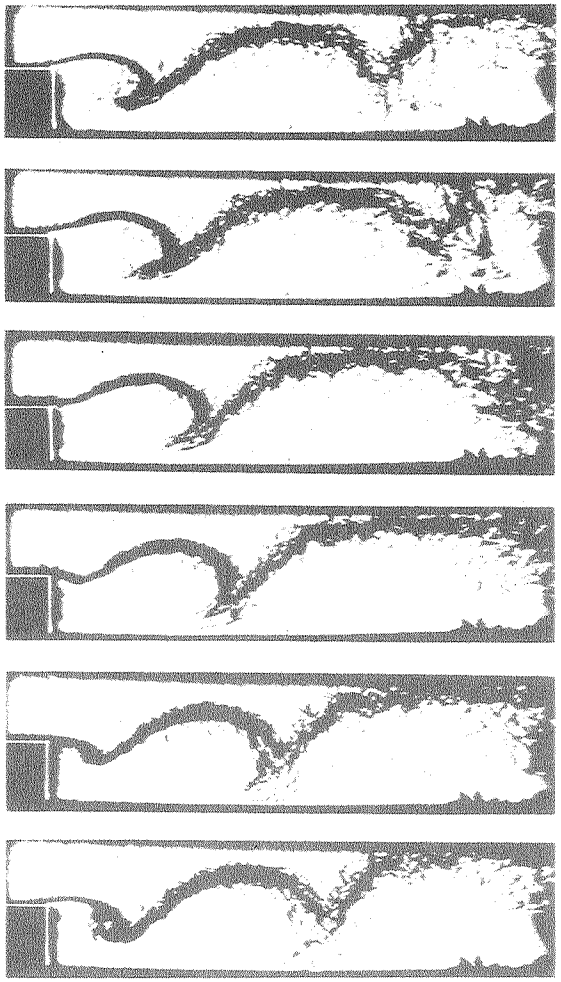

Fig. 1. Cinematographic schlieren record of humming. Equivalence ratio: 0.86. Time interval between frames: 1 msec. (XBB 811-13)

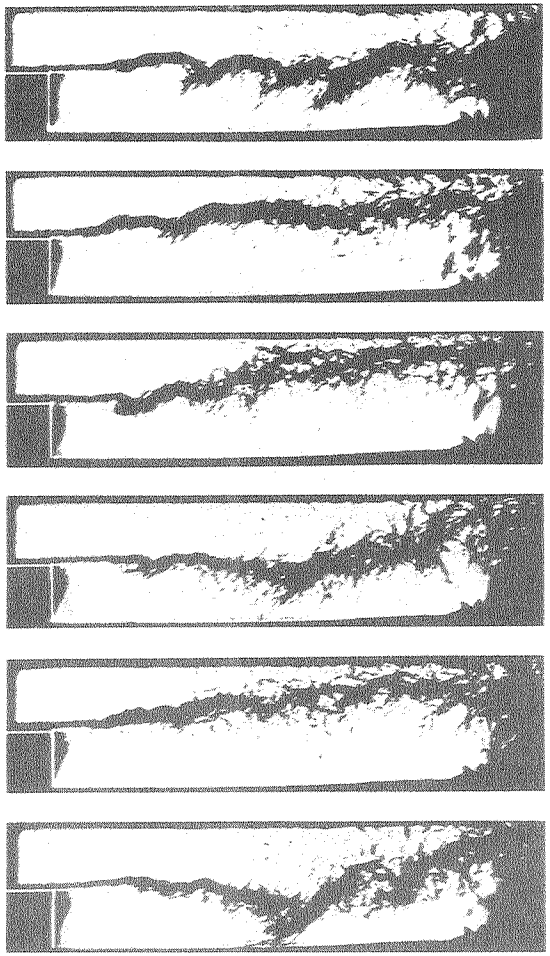

Fig. 2. Cinematographic schlieren record of buzzing. Equivalence ratio: 0.80. Time sequence of frames: 0, 8, 14, 22, 36, 48 msec. (XBB 811-14)

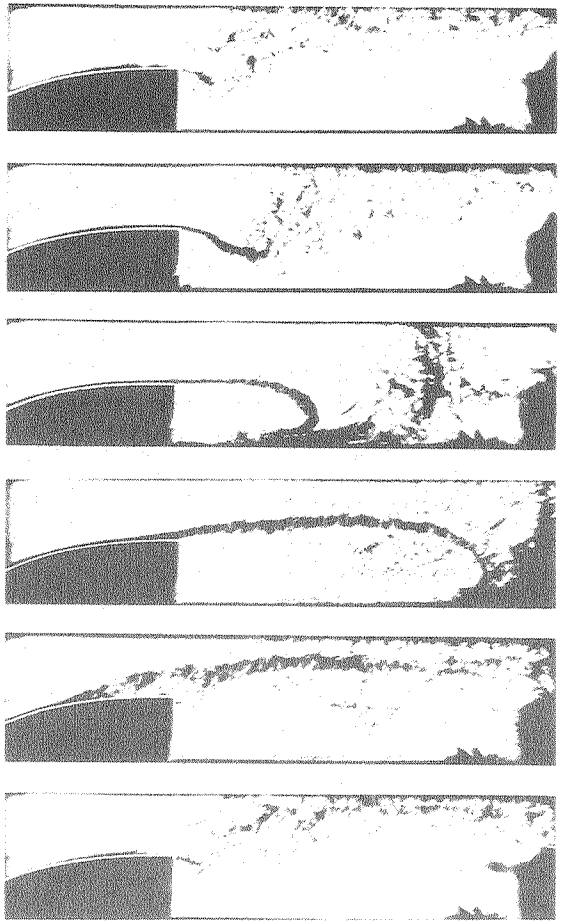

Fig. 3. Cinematographic schlieren record of chucking. Equivalence ratio: 0.85. Time interval between frames: 4 msec. (XBB 811-15)

The first sketch in Figure 4 was deduced from the results of the numerical modeling analysis for stable combustion. The second sketch illustrates the formation of the first vortex in humming displayed in Figure 1. This is evidently caused by the pairing of the recirculation vortex A with the first component of the set of trailing vortices. The next vortex downstream is, in our opinion, the result of the growth of vortex A in the course of its convection. The third sketch describes the reason for the flattening of the flame observed in buzzing (Fig. 2), the stretching due to the combined action of the counter-rotating vortices A and B. The convection of vortex B downstream ushers the pairing between vortices C and D, a relatively rapid process forming vortex A' as it appears in the last sketch of Figure 4. The occurrence of this process does not have to be associated with the propagation of the flame upstream. Thus the repetition of the patterns depicted in the third and the sixth sketches represents the essential features of chucking. Therefore, it is the fast pairing of vortices C and D that produces the pulsing motion of the flame tongue observed in schlieren cinematographic records. The sequence of events illustrated in the fourth and fifth sketches in Figure 4 describes the augmented chucking associated with flashback, the eventual outcome of combustion instabilities -- the major subject of our study.

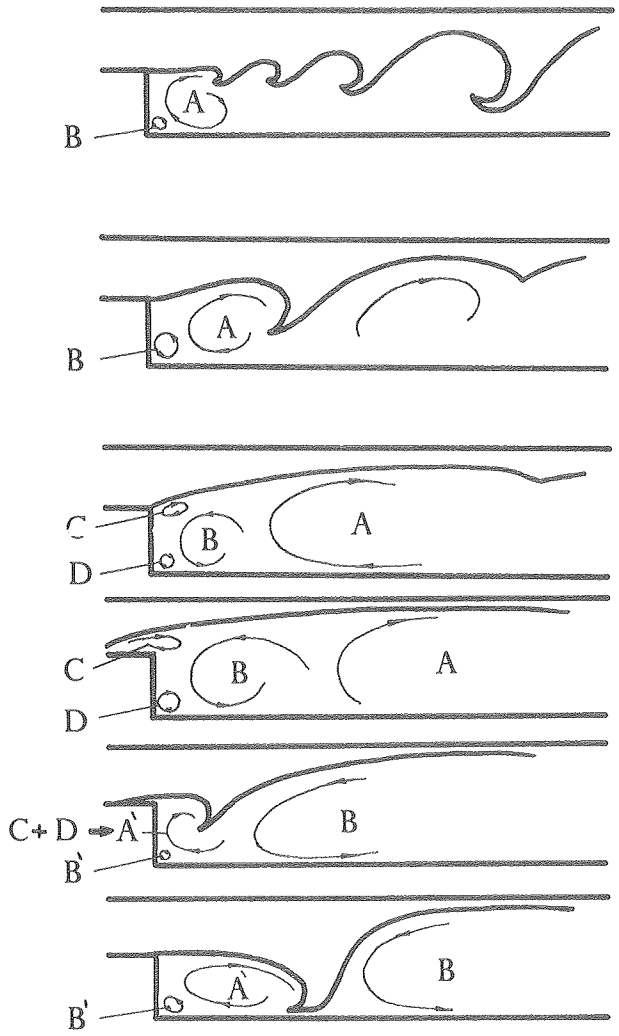

Fig. 4. Sketches of the interactions between the recirculation and trailing vortices deduced from schlieren records and numerical modeling analysis. (XBL 811-7515)

PLANNED ACTIVITIES FOR FY 1981

The observations made above become more meaningful if they are supported by a qualitative analysis. We propose to accomplish this at the next stage by computer experiments carried out by the use of our numerical modeling technique, as described in the article "Numerical Modeling of Turbulent Combustion" elsewhere in this volume. The clarification of the detailed properties of the flow field obtained in this manner should assist designing future combustion tunnel experiments, as well as expanding our studies to include other geometrical configurations of bluff body flame holders in combustors for premixed gases.

REFERENCES

1. A. K. Oppenheim and F. J. Weinberg, "Combustion R&D Key to Our Energy Future," Astronautics & Aeronautics, vol. 12, no. 11, pp. 22-31, (Nov. 1974).

2. A. M. Mellor, "Gas Turbine Engine Pollution," Progress in Energy and Combustion Science, vol. 1, N. A. Chigier, ed.: Pergamon Press, Oxford, pp. 111-133 (1976).

3. L. J. Spadaccini, "Low Emission Combustors for Gas Turbine Powerplants," Combustion Science and Technology, vol. 9, pp. 133-136 (1974).

4. A. H. Lefebvre (Editor), "Lean Premixed/Prevaporized Combustion," U.S. National Aeronautics and Space Administration Report, NASA CP-2016 (Jan. 1977).

5. S. I. Cheng, and A. A. Kovitz, "Theory of Flame Stabilization by a Bluff Body," Seventh Symposium (International) on Combustion, Butterworths Scientific Publications, London, pp. 681-691 (1959).

6. R. E. Jones, L. A. Diehl, D. A. Petrash, and J. Grobman, "Results and Status of the NASA Aircraft Engine Emission Reduction Technology Programs," U.S. National Aeronautics and Space Administration Report, NASA TM-79009 (Oct. 1978).

7. J. B. McVey and J. B. Kennedy, "Lean Stability Augmentation Study," U.S. National Aeronautics and Space Administration Report, CR-159536 (UTRC-914104-18) (1979).

HEAT TRANSFER WITH COMBUSTION*

R. Greif, H. Heperkan, J. Woodard, S. Vosen, D. Wong, and J. Naccache

INTRODUCTION

One of the major goals of this research has been the experimental and theoretical determination of the temporal variation of the heat flux during compression and combustion processes. This is of considerable practical importance and is also of fundamental interest. With respect to internal combustion engines, heat transfer processes are critical to: quenching of wall reactions which cause high hydrocarbon emissions, the loss of energy which results in decreased efficiency, and the durability of engine components.

Measurements have been made in a single pulse, compression expansion apparatus that was built by Oppenheim, et al.[1] to study reciprocating engine processes under well-controlled laboratory conditions which simulate the operation of a spark-ignition engine. Completed studies in the apparatus include the experimental and theoretical determination of the unsteady wall heat transfer in non-reacting gases during piston compression.[2,3]

Measurements in the presence of reacting gases have been made in a shock tube and in a constant volume combustion chamber.[4] These studies are of general interest and provide an introduction to the study of more general phenomena concerning combustion during piston compression.

ACCOMPLISHMENTS DURING FY 1980

Measurements to determine heat transfer during combustion were made previously in non-reacting gases with a thin film resistance thermometer. The resistance thermometer, consisting of a thin platinum film on an insulted backing, is connected as the active element in a dc bridge. An increase in surface temperature causes a change in resistance of the platinum film. The measured variation of the resistance as a function of time yields the desired wall temperature variation.

Using these measurements, the temporal variation of the wall heat flux may be obtained when the resistance thermometer is mounted flush with the wall. The result is derived by solving the conduction equation in the solid wall (insulated backing), subject to the measured variable surface temperature. The heat flux is expressed as a Duhamel integral in terms of the variable surface temperature and the wall properties. The validity of this measurement and analysis has been demonstrated in our previous publications.[2,3]

An alternative, independent approach for determining of the wall heat flux is the solution of the conservation equations in the gas to obtain a heat flux based on the gas properties. Good agreement has been obtained for the two heat fluxes in the following experiments: (a) during piston compression in the single pulse apparatus, and (b) during shock wave compression in a shock tube.

When reactions occur, the gas dynamic and transport phenomena are complex. For this condition, the measured heat flux is used to determine fundamental results concerning combustion phenomena. These measurements have been made in a shock tube where a mixture of hydrogen, oxygen and argon was ignited due to shock wave heating. New results include the temperature distribution in the gas at different times (Fig. 1). The wall location corresponds to the zero value of the abscissca with ignition commencing at 20 μsec.[4] Another important result is the location of the combustion zone as a function of time. The analysis shows that the zone moves toward the wall and then remains, for a considerable time, at a fixed, quenching distance from the wall.[4]

Another study with reacting gases has been initiated in a constant volume chamber with a methane air mixture. Experiments were performed in a steel explosion vessel that was fitted with optical glass windows suitable for schlieren photography. The mixture was ignited by a spark and the flame that formed propagated toward the wall which contained a resistance thermometer. In preliminary measurements, the temporal variation of the wall heat flux was obtained and photographs were also taken of the advancing flame front.

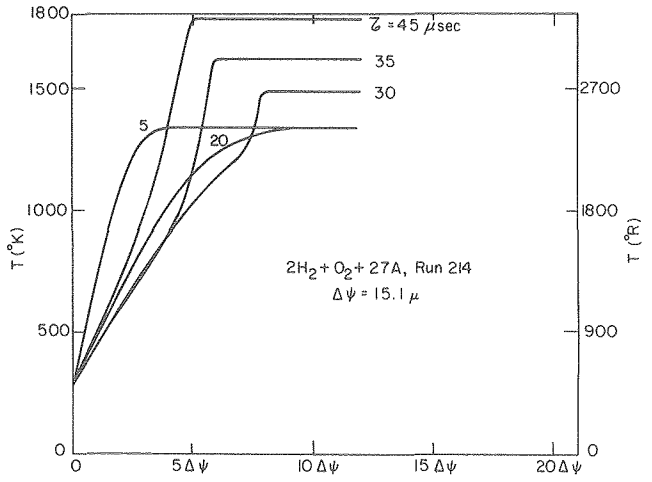

Fig. 1. Gas temperature distribution.
(XBL 806-10302)

* This work was supported by the Assistant Secretary for Conservation and Solar Energy, Office of Transportation Programs, Transportation and Energy Conservation Division of the U.S. Department of Energy under Contract No. W-7405-ENG-48.

PLANNED ACTIVITIES FOR FY 1981

Experiments in the constant volume chamber and analysis of the fluid flow and energy transport associated with the advancing flame front will be continued. This work follows as a natural outgrowth of previous shock tube studies. In addition, studies will be made in the two single pulse compression expansion facilities. In particular, experiments and analyses of the roll-up vortex, piston expansion, and combustion phenomena will comprise this part of the research.

REFERENCES

1. A. K. Oppenheim, R. K. Cheng, K. Teichman, O. I. Smith, R. F. Sawyer, K. Hom, and H. E. Stewart, "A Cinematographic Study of Combustion in an Enclosure Fitted with a Reciprocating Piston," in Stratified Charge Engines, Institution of Mechanical Engineers Conference Publications 1976-11, pp. 127-135 (1976).

2. M. Nikanjam and R. Greif, "Heat Transfer During Piston Compression," Transactions of the ASME, J. of Heat Transfer, vol. 100, p. 527 (1978), and Lawrence Berkeley Laboratory Report LBL-7338.

3. R. Greif, T. Namba, and M. Nikanjam, "Heat Transfer During Piston Compression Including Side Wall and Convection Effects," International J. of Heat and Mass Transfer, vol. 22, pp. 901-908 (1979).

4. H. A. Heperkan, "An Experimental and Theoretical Study of Heat Transfer with Combustion," Ph.D. Dissertation, University of California, Berkeley (1980) and Lawrence Berkeley Laboratory Report LBL-10868.

ENGINE COMBUSTION STUDIES*

R. Sawyer, J. Daily, A. Oppenheim, and H. Stewart

INTRODUCTION

Development of efficient and environmentally benign internal combustion engines depends to a large extent on the attainment of their reliable operation, using premixed, lean mixtures. Studies of lean combustion processes pertaining to this objective have been conducted in our laboratory by the use of a single-pulse, compression-expansion machine. This unique facility, which we developed, features a square piston between two windows, permitting an unobstructed optical access to the entire chamber where combustion takes place, under conditions similar to those existing in reciprocating piston engines.

In the initial version of the machine, the piston was pneumatically driven and hydraulically controlled. This version had a number of drawbacks, the most important being the difference of the piston trajectory from that of a reciprocating piston engine.

Nonetheless, the pneumatically operated prototype has been used successfully to investigate piston induced flow fields, valve generated turbulence, ignition processes, flame structure and propagation, bulk and wall quenching, and time-resolved heat transfer phenomena.

On the basis of experience gained, an improved version of the machine has been designed and constructed. Its major features are:

1. The piston is driven by a crankshaft, and its motion is controlled by a fast acting clutch-brake mechanism, permitting one, two, three, or four stroke operation.

2. The cross-section of the combustion chamber is larger and has the same area as a standard CFR laboratory test engine.

3. The head is provided with conventionally operated overhead intake and exhaust valves.

ACCOMPLISHMENTS DURING FY 1980

The crankshaft operated compression-expansion machine has been assembled and provided with controls and a computerized data processing system, as schematically described in Figure 1. Basically, the computer has the capability to control the operation of the machine and the acquisition and reduction of data. However, at this stage, these facilities have not yet been put into operating condition, and the cylinder head, fitted with solenoid actuated valves indicated in Figure 1, is not yet available.

PLANNED ACTIVITIES FOR FY 1981

Initially, we intend to use the apparatus for the study of the local consumption of fuel by making time resolved measurements of methane concentration, using absorption at 3.39 μ m with an

* This work was supported by the Assistant Secretary for Conservation and Solar Energy, Office of Transportation Programs, Transportation Energy Conservation Division of the U.S. Department of Energy under Contract No W-7405-ENG-48.

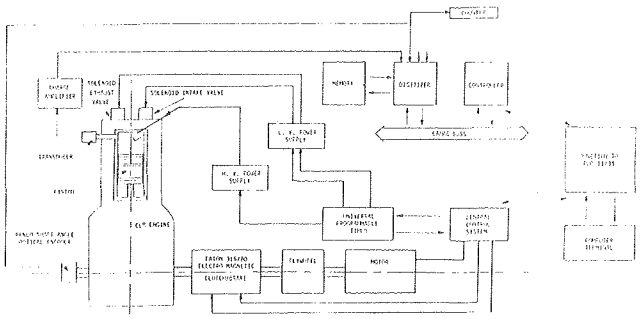

Fig. 1. Schematic diagram of the crank-operated compression-expansion machine with a computerized control and data processing system. (XBL 811-7563)

Ne-He laser as the light source. Figure 2 shows the test section of the apparatus with the laser system in place. The optical arrangement of the method is depicted on the photograph by the light beam that has been traced with the use of the alignment laser.

Upon the completion of this preliminary investigation, we plan to use the machine for a comparative study of ignition systems, with particular attention given at first to plasma jet ignition in comparison to a conventional spark plug. At the same time, work will be in progress on the introduction of computer monitored operation of the apparatus and data processing system.

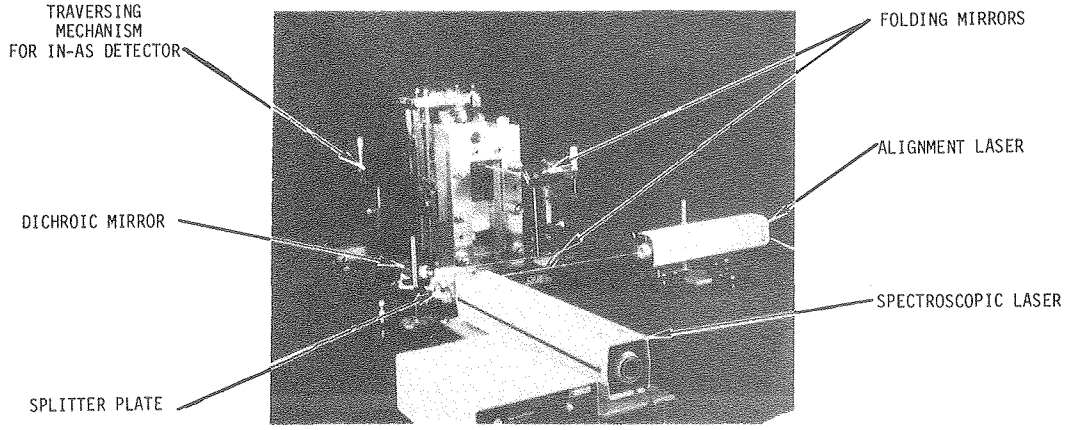

Fig. 2. Test section of the crank-operated compression-expansion machine with laser instrumentation for time-resolved measurement of methane concentration by absorption at 3.39 μm. (XBB 811-438)

IGNITION STUDIES*

A. Oppenheim, F. Hurlbut, F. Robben, R. Peterson, P. Coico, and H. Stewart

INTRODUCTION

It had become increasingly apparent that work on the fundamental science of combustion processes in lean mixtures, specifically work on lean mixture ignition processes, would be greatly advanced through the methods of direct molecular beam mass sampling. It was envisioned that a suitable system to accommodate the simultaneous coordination of optically based diagnostic observations would include high speed schlieren photography, emission and absorption spectroscopy, and laser fluorescence. Accordingly, our objective has been development of a system for time-resolved mass analysis which would lend itself easily to the accommodation of the peripheral instrumentation.

Funding for this program of study became effective at the end of 1978, and preliminary design was initiated by January of 1979. Fabrication of primary elements of the vacuum shell and support frame was completed in FY'79.

ACCOMPLISHMENTS DURING FY 1980

Major effort was devoted to the continuing construction and development of the molecular beam system. Construction and installation of the essential elements of the vacuum shell and its instrumentation were accomplished during the winter of 1979. In April 1980, the system was placed under evacuation by diffusion pumps. By May, following final minor modifications, a system base pressure of 5×10^{-7} Torr was reached. Preliminary tests in June verified that all regions of the beam system were at design pressures or lower, under the design beam load.

During the spring of 1980, installation of the mass spectrometer[1] and related system components was started. By late June, preliminary tests of molecular beam and mass spectrometer functions were made to determine acceptable mass resolution and signal sensitivity.

We selected the CAMAC design approach for function control and instrumentation housing to serve the substantial number of controlled mechanical and electronic system elements eventually required. A resident dedicated computer will be used to control essential functions, including the precise timing of events and the recording and analysis of data. A standard Engineering MIK-11 computer, housed in the CAMAC "crate", would serve for system function sequencing, data acquisition, and preliminary processing. The LBL Real Time Measurements Group acquired and assembled the basic system and provided it with essential operating programs. It was delivered to the main system by May 1980 and was then combined with a fast ATD converter. Subsequently, in early June, during a check of computer system function, the pressure history of methane-air ignition was digitized and recorded. Entirely satisfactory agreement was observed between the digitized record and oscilloscope photographs.[2] Two other electronic components essential to computer controlled system operation were received by the close of FY'80: the precision (16 bit) DTA converter for setting spectrometer mass number and the clock controller for operations sequencing. The remainder of FY'80 was occupied with continued system development, including installation of the molecular beam modulator, the timing signal system, and the back-to-air back-fill system, as well as refinements to the calibration source and associated pressure instrumentation.

System Overview

The cross-section of the molecular beam apparatus is displayed in Figure 1. Shown in Figure 2 is a functional schematic diagram of the associated control system. The apparatus consists of several sub-systems which may be identified according to function:

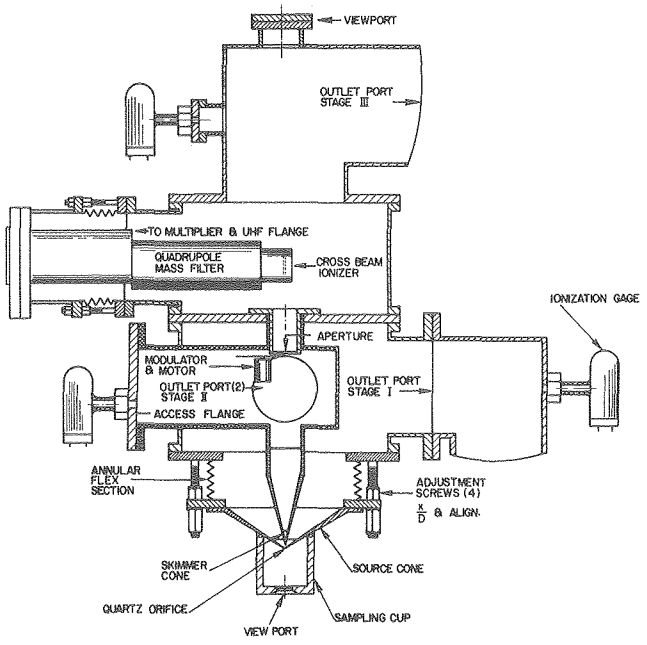

Fig. 1. Cross-section of the molecular beam shell. (XBL 811 7513)

* This work was supported by Director, Office of Energy Research, Office of Basic Energy Sciences, Engineering, Mathematics, and Geosciences Division of the U.S. Department of Energy under Contract No. W-7405-ENG-48.

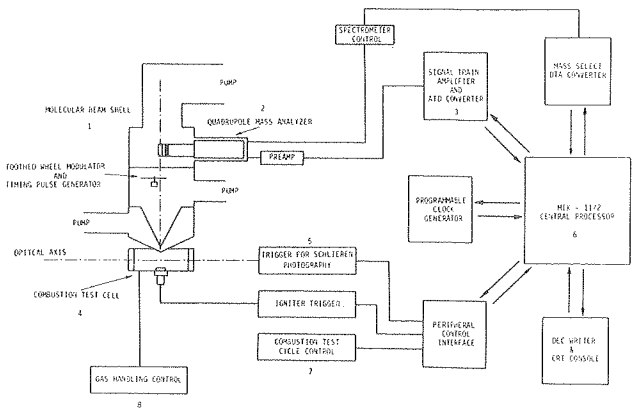

Fig. 2. Functional schematic diagram of molecular beam mass sampling system. (XBL 811 7514)

Fig. 3. General view of molecular beam mass sampling system. (CBB 803 3319)

1. Molecular beam, consisting of the sampling source, skimmer, modulator with timing signal generator, associated vacuum pumps, gauges, and controls.

2. Quadrupole mass analyzer, consisting of ionizer, analyzer, particle detector, R. F. power supply, High-Q head, ionizer control, and quadrupole control.

3. Signal train, consisting of *preamplifier, *voltage amplifiers, and fast ATD converter.

4. **Test cell and igniter.

5. *Flash schlieren (optic axis only shown).

6. Central processor, consisting of MIK-II mini-computer with DEC writer and scope monitor, *clock controller, *mass select DTA converter, and **peripheral control interface.

7. **Cycle controller for combustion test cell and igniter.

8. **Combustion cell, calibration gas supply, and metering system, including calibration source cell.

Items marked with an asterisk (*) are under development while those marked with two asterisks (**) are yet to be designed or acquired. In addition (not shown), a synchronous detector and waveform educator have been installed to assist with the initial calibration.

General views of the apparatus are shown in Figures 3 and 4. In Figure 3, spectrometer components and the MIK-11 computer are on the right; vacuum control and monitoring components are on the left, and the molecular beam shell is at the upper center. Figure 4 is a side view of the molecular beam shell, showing the outer end of the spectrometer at upper left center and lower center, depicting the clear optical path past the sampling path.

PLANNED ACTIVITIES FOR FY 1981 and FY 1982

For the next year we will be engaged in experimental work designed to give needed information on system function and, in its later phases, on system performance with respect to time-resolved analysis

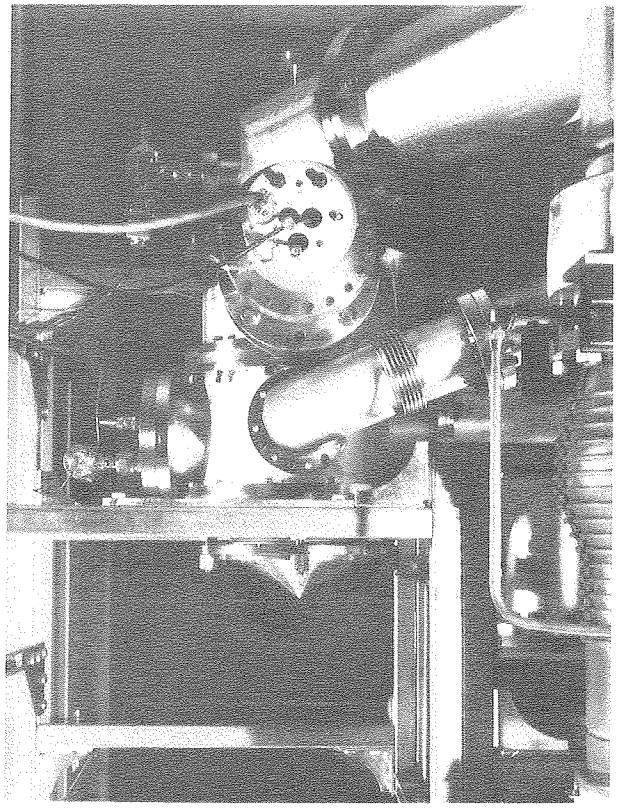

Fig. 4. Side view of molecular beam system showing sampling cone. (CBB 803 3317)

of active radical production. The program of this work will be:

1. A series of time resolution, calibration experiments for various permanent gases will be performed using the disc modulator with narrow slots. This will be used to demonstrate full system functional capability. At the same time, beam intensity measurements will give needed information on system sensitivity. This will enable a detailed rationalization of the beam performance of this instrument. Information developed in these studies is essential to the next phases of the program and for completion of a system documentation report now in preparation. Estimated completion date: January 1981.

2. Detection of active radicals will be first demonstrated in studies of hydrogen peroxide (H_2O_2), using flash photolysis. This method for the production of radicals was actively studied in the 1950's[3] complementing the time-history information obtained by absorption and emission spectroscopy.[4] Because of the relative simplicity of the chemical system, it is expected that quantitative calibration can be achieved. At the same time, useful new information concerning rate constants in this system can be derived. Estimated completion date: end of FY'81.

3. We envision next the studies of transient thermal ignition of H_2 and of other gases at the surfaces of catalytic and non-catalytic ribbons. This work will also produce spectrometer-calibration information and new rate-constant information. Completion date: mid- to end-FY'82.

4. The foregoing work will, to a degree, be coincident with development and preliminary experimentation studies of plasma and combustion jets and jet-stimulated ignition. Although the broad scope of this work makes a detailed projection inadvisable at this time, we expect some portion of the work on plasma jets to be completed by the end of FY'82.

REFERENCES

1. Extra Nuclear Laboratories, Inc.

2. R. Peterson "Application of Analog-to-Digital Converter to Data Gathering" ME249 Project Report.

3. R. G. W. Norrish, "The Study of Combustion by Photochemical Methods" Tenth Symposium (International) on Combustion, pp. 1-18, The Combustion Institute (1965).

4. C. Birkby and E. Hutton, "Gaseous Explosions Initiated by Flash Photolysis - An Investigation of Radical Ion Formation," Thirteenth Symposium (International) on Combustion, pp. 767-775, The Combustion Institute (1971).

COMBUSTION CHEMISTRY AND POLLUTANT FORMATION

MEASUREMENT OF NITROGENEOUS POLLUTANTS IN COMBUSTION ENVIRONMENTS*

D. Lucas, N. Brown, and A. Newton

INTRODUCTION

Combustion systems that employ synthetic or fossil fuels are often faced with problems associated with high concentrations of chemically bound nitrogen and sulfur. The assessment of health and environmental effects of combustion generated pollutants and research into pollution control techniques are handicapped by a lack of analytical techniques that can accurately determine the types and amounts of nitrogen and sulfur compounds present in post-combustion environments.

Research in this area has been directed to the detection and measurement of nitrogenous species, with emphasis on ammonia measuring techniques. Ammonia measurements are of particular interest because some NO control technology employs NH_3 to selectively reduce NO in post-combustion gases.

Ammonia concentrations in combustion systems are currently measured by a variety of techniques.[1] We have developed a technique, based on the sodium phenolate method, that can accurately and reproducibly measure NH_3 in combustion exhausts over a wide range of concentrations and combustion conditions.[2]

* This work was supported by the Assistant Secretary for Environment, Office of Environmental Compliance, Division of Environmental Safety and Engineering of the U.S. Department of Energy under Contract No. W-7405-ENG-48; by the Morgantown Energy Research Center of the U.S. Department of Energy under Contract No. PR-14037; and by the California Air Resources Board under contracts No. A6-196-30 and No. A8-146-31.

We have compared two of the more commonly used methods with our technique to determine what errors and interferences arise from their application to combustion research.

All of the sampling was done in a laboratory combustion tunnel fired with light fuel oils which could be doped with prototype fuel nitrogen compounds. Identical uncooled-quartz sampling probes and Teflon transfer lines were used in all systems to eliminate differences due to probe effects.

ACCOMPLISHMENTS DURING FY 1980

The sodium phenolate method was developed specifically to measure NH_3 in combustion exhaust gases. The collection system consists of glass U-tubes in series, the tubes filled with phosphoric acid coated glass beads. The sampling manifold is designed to eliminate the problem of water and/or ammonia condensation elsewhere in the system. Measurements indicate that recovery of NH_3 is in excess of 95% in the first tube. After collection, the ammonia is transferred to a flask by washing. Here it is chlorinated and subsequently reacted with sodium phenolate to form an indophenol dye. The optical density of the dye is measured at its absorption maximum, 632 mm. Numerous tests confirm that the NH_3 is quantitatively collected, transferred, and converted to the dye, and that only low molecular weight primary amines could possibly interfere in the analysis. Using this method, absolute errors to sample combustion exhausts are estimated to be less than 10%. While the method gives excellent results, it may not gain widespread use because of its low sampling rate and relatively long analysis time. It is particularly useful as a reliable standard to determine if other methods yield consistent results.

Perhaps the most convenient way of measuring NH_3 is to oxidize it to NO in a catalytic converter, followed by NO detection in a chemiluminescent analyzer. This method suffers mainly in that most NO analyzers are not equipped to handle the high concentrations of water vapor present in combustion exhausts, and there is interference from any nitrogenous species that can be oxidized to NO in the converter. Condensation of water anywhere in the system can lead to large errors because of the high solubility of NH_3. In addition, NH_3 can be adsorbed on many surfaces. To avoid these problems, a TECO Model 12 chemiluminescent analyzer was modified to eliminate condensation. The conversion efficiency of NH_3 to NO over a stainless steel catalyst was measured as a function of both temperature and NH_3 concentration; the results are presented in Figures 1 and 2. Table 1 is a comparison of NH_3 concentrations measured by the sodium phenolate and the NO_x method for a variety of combustion conditions. The NH_3 concentrations measured by the chemiluminescent method have been corrected for the vapor concentration. Corrections for CO_2, H_2O, and O_2 quenching of NO^* are estimated to be less than 5% for the conditions studied. In lean combustion systems, the NO method can be successfully used to measure NH_3 concentrations as long as other nitrogenous species such as NO_2 or HCN are not present in large amounts. The accuracy of this method is estimated to be $\pm$10%, the same as for the sodium phenolate method. It

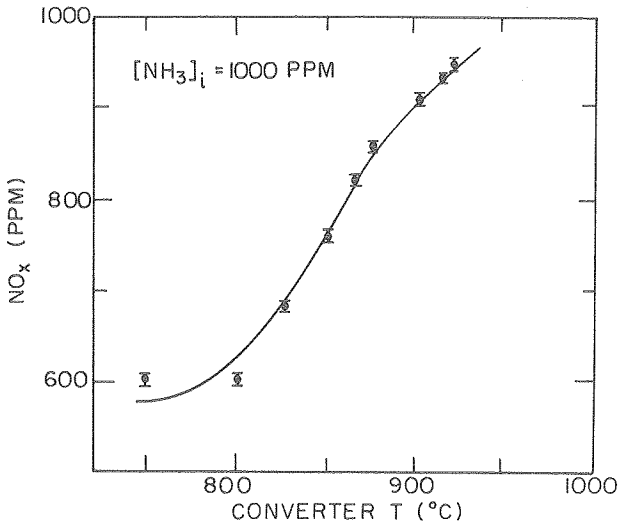

Fig. 1. NH_3 to NO conversion efficiency as a function of temperature of a stainless steel catalyst. (XBL 8012-13386)

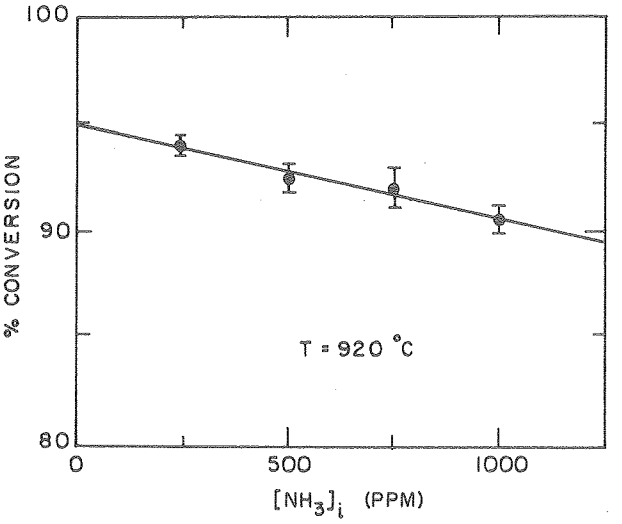

Fig. 2. NH_3 to NO conversion efficiency as a function of NH_3 concentration. (XBL 8012-13383)

Table 1. NH_3 Measurements.

T(K)	ϕ	NO (ppm)	NH_3 (ppm) NO_x Method	NH_3 (ppm) Phenolate Method
1100	.83	320	677	653
1169	.95	117	318	352
1229	.78	29	340	362
1233	.74	265	27	32
		31	249	274
1235	.73	350	8	12
		49	2	1

should be noted that low (less than 0.1%) concentrations of fuel sulfur did not poison the catalyst.

The third method of analysis employs a specific ion electrode, which uses a hydrophobic gas-permeable membrane to separate the sample from an internal solution. Dissolved ammonia diffuses across the membrane where it can react with the internal solution: $NH_3 + H_2O \leftrightarrows NH_4^+ + OH^-$. The electrode is sensitive internally to the OH^- concentration, which is proportional to the NH_3 concentration in the sample. Ammonia is often collected by bubbling exhaust gases through a weak solution of sulfuric acid. The NH_3 can be collected quantitatively, but the CO_2 that dissolves in the solution can lead to a 20% absolute error in the electrode potential. This is due to two factors: the CO_2 acts as an acid, altering the pH of the solution and the effect of the dissolved species (including HCO_3^- and $CO_3^=$) which changes the ionic strength of the solution, which in turn effects the partial pressure of NH_3. Although this interference may be well known to electrochemists, it has not been characterized for combustion applications. The collection technique developed for the sodium phenolate method works well for the ion analysis and is especially attractive due to the small liquid volumes employed, which reduces the CO_2 interference problem. With no CO_2 interference, the electrode works as well as the sodium phenolate method. However, it suffers from a larger amine interference and is also somewhat plagued by an arduous analytical procedure.

PLANNED ACTIVITIES FOR FY 1981

Techniques for measuring NH_3 in the presence of other nitrogenous species and rich combustion environments will be examined. Hydrogen cyanide detection in combustion exhaust will be measured by at least three techniques: gas chromatography, cyanide specific ion electrodes, and Kitagawa - type gas detectors. Analytical procedures for measuring sulfur compounds in post-combustion environments will also be characterized.

REFERENCES

1. Examples of the techniques used are direct neutralization, infrared analysis using conventional spectrometers and laser diodes, UV absorption, and Nessler tubes.

2. D. Lucas, A. S. Newton, and N. J. Brown, "The Measurement of NH_3 in Combustion Environments." In preparation.

THE SELECTIVE REDUCTION OF NO BY NH_3*

D. Lucas, N. Brown, and R. Sawyer

INTRODUCTION

Photochemical smog, nitrogen dioxide and other potentially harmful nitrogenous species in the atmosphere can be significantly reduced by controlling nitrogen oxide emissions from combustion sources. Different control processes to achieve a reduction in nitrogen oxide emissions are under consideration, including combustion modification and/or staging and the use of low nitrogen content fuels. Other processes, rather than limiting the formation of NO during combustion, allow NO to form and selectively eliminate it through chemical reactions in the post-combustion gases. Our research is concerned with characterizing the selective, homogeneous reaction of NO with NH_3 in the post-combustion environment of prototype oil fuels. The selective reduction was first described by Lyon and Longwell.[1] This approach appears promising because it can be used in a variety of combustion systems and is not dependent upon the formation mechanism of NO.

The reduction of NO by NH_3 is being studied in a laboratory scale combustion tunnel which allows good control over a range of experimental conditions. The tunnel is approximately 3.5 m long, with an internal diameter of 5 cm over most of its length. It consists of three major parts: a combustion section, an ammonia injection region, and a reactor region where the selective reduction occurs. Complete, stable, and reproducible burning of a fuel/oil/air mixture is accomplished in the first section. The fuel, a light diesel oil with a hydrogen/carbon ratio of 1.85, is injected through a high pressure atomizing nozzle into a metered air stream. Rapid mixing and combustion stabilization is accomplished with baffles and blockage disks. Fuel nitrogen is simulated by admixing NO to the air supply or by mixing small amounts of pyridine with the fuel oil. The temperature of the products of combustion exiting this section is controlled by water cooling of the combustor walls, and achieves a specified value T* immediately prior to the ammonia injectors. A mixture of NH_3 and N_2 is introduced through four symmetrically placed quartz injectors and admixed rapidly with the products of combustion. Composition and temperature profiles in both the axial and radial directions are measured in the reactor section. Samples are withdrawn for analysis through quartz sampling probes at four locations downstream of the ammonia injection.

* This work was supported by the U.S. Department of Energy under Contract No. W-7405-ENG-48 and by the California Air Resources Board under Contracts No. A8-146-31 and No. A6-196-30.

Conditions are such that uniform radial composition profiles are obtained quickly, with the NH_3 - NO reaction essentially complete (>95%) by the final probe station. The survival of NO is determined as a function of equivalence ratio, the source and initial concentration of NO, the temperature at the ammonia injection, and the amount of NH_3 added to the combustion gases. Concentrations of CO, CO_2, NO_x, NH_3, HCN, H_2O, and O_2 are measured by a variety of techniques, including continuous gas analyzers, wet chemical methods, and gas chromatographs. The NH_3 concentration remaining after 95% or greater reduction is termed ammonia breakthrough.

ACCOMPLISHMENTS DURING FY 1980

Nitric oxide reduction by NH_3 addition has been studied at three equivalence ratios (ϕ = 0.78, 0.83, and 0.95) as a function of temperature and the amount of added NH_3 ($\beta = [NH_3]_i/[NO]_1$). Figure 1 shows the NO reduction and NH_3 breakthrough measured at a fixed temperature and equivalence ratio. This behavior is observed over the entire range of conditions studied. As more ammonia is injected, more NO reduction occurs, even at β values greater than 4.0. As expected, the ammonia breakthrough increases with increasing β. These results are consistent with previous investigations[2,3,4], despite their use of different fuels and NO sources. No significant difference in the NO reduction was observed when pyridine was burned as the source of NO, rather than directly injecting NO gas into the air supply.

Determination of the temperature at which maximum NO reduction occurs at a fixed equivalence ratio is shown in Figure 2. At a constant ϕ, the

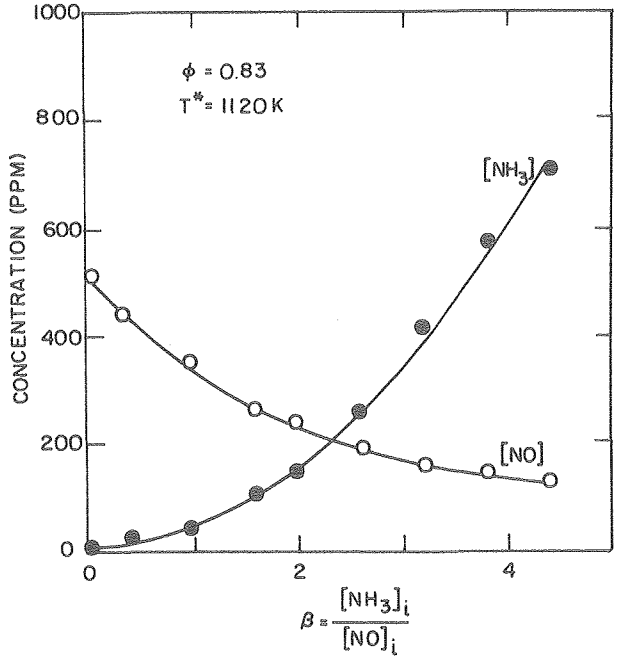

Fig. 1. Nitric oxide and ammonia concentrations as a function of β at a constant temperature equivalence ratio and ammonia injection temperature.
(XBL 8012-13387)

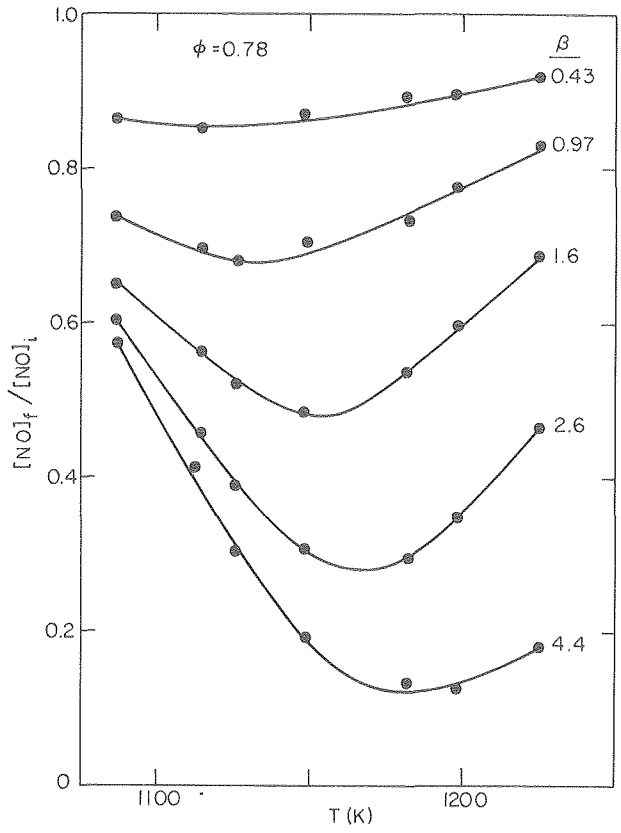

Fig. 2. The NO survival, $(NO)_f/(NO)_i$, as a function of β. The equivalence ratio is 0.78.
(XBL 8012-13384)

temperature for optimum NO reduction increases with increasing β. The relationship between the optimal reduction temperature and β changes when the equivalence ratio is altered, becoming more pronounced at lower levels of ϕ. Additional data also indicate that at a fixed β value, the optimum temperatures increases with ϕ. Our studies indicate that the temperature for maximum NO reduction varies rather significantly from about 1120 K to 1200 K for conditions investigated.

Ammonia breakthrough measurements are presented in Figure 3. It appears that the temperature and the relative amount of NH_3 injected are the only factors that determine the concentration of NH_3 which remains after reaction. The problem of ammonia breakthrough can thus be minimized by operating at conditions of high NH_3 injection temperature and low β values. It should be noted that the importance of the ammonia breakthrough in terms of health and environmental effects has not been established.

Numerous attempts were made to detect and quantify the presence of other "odd nitrogen" species, including NO_2, HCN, and higher amines. With no NH_3 addition, up to 2 parts per million of a nitrogenous compound, presumed to be NO_2, capable of being converted to NO in a stainless steel catalytic converter at 920 C, was observed when the fuel oil was doped with pyridine. However, no HCN or amines were detected by other independent methods at any of the conditions used

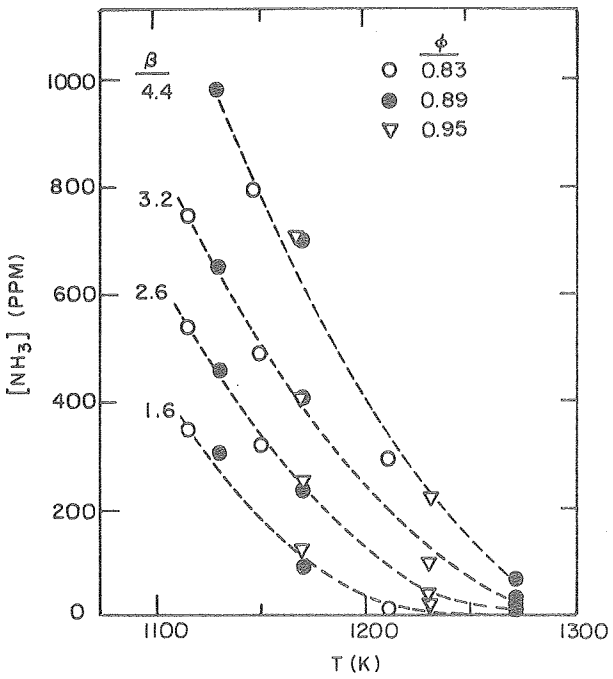

Fig. 3. Ammonia breakthrough measurements as a function of the ammonia injection temperature. (XBL 8012-13385)

in this study. A conservative upper limit of a few parts per million can be set for the total concentration of odd nitrogen species other than NH_3 and NO.

In practical applications, utilization of the selective reduction of NO by NH_3 requires monitoring temperature, excess oxygen, NO, and NH_3 to insure maximum reduction. The trade-off which exists in terms of nitric oxide emissions and ammonia breakthrough necessitates the development of techniques that reliably measure NH_3 in combustion exhaust environments. Another possible alternative is to remove the remaining NH_3 from the exhaust gases, either catalytically or through homogeneous reactions.

PLANNED ACTIVITIES FOR FY 1981

Current research centers on the role of sulfur compounds in the selective reduction of NO. Thiophene and pyridine doped fuel oil will be used as a prototype fuel that contains high concentrations of both fuel nitrogen and fuel sulfur. Analysis of SO_2 in the product gases with a fluorescent detector will help determine if synergistic effects between sulfur and nitrogen compounds are important in the NO reduction process.

REFERENCES

1. R. K. Lyon and J. P. Longwell, "Selective Non-Catalytic Reduction of NO_x with NH_3," EPRI NO_x Control Technology Seminar, San Francisco, California (1976).

2. T. S. Eitzen, N. J. Brown, A. S. Newton, A. K. Gordon, and K. S. Basden, "Characterization of NO_x Removal Through Ammonia Addition," Western States Section, The Combustion Institute Paper No. 79-22 (1979). Also Lawrence Berkeley Laboratory Report LBL-8849 (1979).

3. N. J. Brown, R. F. Sawyer, and T. S. Eitzen, "Characterization Studies of the Selective Reduction of NO by NH_3." Final report submitted to the State of California Air Resources Board. Lawrence Berkeley Laboratory Report LBL-10254 (1979).

4. L. J. Muzio, J. K. Arrand, and D. P. Teixeira, "Gas Phase Decomposition of Nitric Oxide in Combustion Products," Sixteenth Symposium (International) on Combustion, The Combustion Institute, Pittsburgh, 199-208 (1977).

REDUCTION OF NO BY COMBUSTION STAGING*

N. Brown, J. Brunetto, D. Lucas, and R. Sawyer

Combustion sources of the mobile and stationary types are largely responsible for the emissions of the nitrogen oxides, NO and NO_2, into the atmosphere. Two mechanistic paths are responsible for NO production during combustion of lean and near stoichiometric mixtures; one involves the oxidation of atmospheric nitrogen (thermal NO), and the other results in NO production from the oxidation of nitrogen chemically bound to fuel molecules (fuel NO). In the combustion of fuels with nitrogen content in excess of 1% by weight, the two mechanisms contribute equally to NO production. Many coals, coal-derived fuels, and shale oil have nitrogen concentrations in excess of 1%. Reductions of NO emissions from the combustion of high nitrogen content fuels are more difficult to achieve because the fuel and thermal NO formation mechanisms, which operate simultaneously, depend differently on experimental variables (e.g., temperature and residence time).

Staged combustion is an abatement technique that appears capable of achieving significant reductions of NO while also minimizing emissions of criteria and non-criteria pollutants. Staged

* This work was supported by the Assistant Secretary for Fossil Fuels, Office of Utilization of the U.S. Department of Energy under Contract No. W-7405-ENG-48 and by the Morgantown Energy Technical Center of the U.S. Department of Energy under Contract No. PR-14037.

combustion divides the overall combustion process into two or more stages to prevent the formation of noxious pollutants. Experimental variables which differentiate one type of staging from another are: (1) the number of stages, (2) equivalence ratio of each stage, (3) residence time associated with each, (4) fuel properties, and (5) nitrogen content.

Our current research program uses innovative and characterizing staging methods suitable for achieving NO reductions during the combustion of fossil fuels with a significant nitrogen content. The program uses two different kinds of laboratory scale combustion experiments. Staged combustion has been investigated in a combustion tunnel suitable for studying turbulent combustion under a variety of experimental conditions. A fluidized bed combustion facility, under construction, will also be used in staging studies. Additional research effort concerns development of analytical techniques suitable for quantifying pollutant emissions under various experimental conditions. This research is described elsewhere in this report.

ACCOMPLISHMENTS DURING FY 1980

The combustion tunnel used in this research is a turbulent flow reactor capable of supporting three combustion stages. This tunnel, modified during FY80 to achieve complete, stable, reproducible burning of liquid fuel sprays, is illustrated schematically in Figure 1. A pressurized liquid fuel delivery system and a nozzle assembly were installed, and a larger combustion section was added to provide a longer residence time in the first stage. The upstream air supply and exhaust sections are packed with steel wool to eliminate accoustic feedback. Fuel/air mixing is achieved by proper positioning of slotted and perforated disks upstream of the flame. Wrapping the primary combustion section with copper cooling coils provides temperature control in the second and third stages. Radial and axial composition and temperature profile measurements indicate that combustion is steady state and reproducible from day to day. Axial temperature gradients in the second stage are approximately one Kelvin per centimeter.

Nitric oxide reduction has been investigated as a function of first and second stage equivalence ratios and temperature. The first stage is fueled by diesel oil admixed with 7% by volume pyridine; the equivalence ratio of this stage varies between 0.73 and 0.87. Nitric oxide levels in the absence of staging are between 540 and 600 ppm, which corresponds to 50% conversion of the fuel nitrogen to nitric oxide. The second stage fuel, propane, is introduced into the first stage exhaust through four symmetrically oriented quartz injectors. The oxygen concentration, calculated after the first stage has been completed, is used with the added propane concentration to determine the equivalence ratio for the second stage. The first and second stage equivalence ratios are both on the lean side of stoichiometric, and the net equivalence ratio is increased by propane addition. For propane addition, reduction of NO is achieved under certain experimental conditions. Illustrative results are shown in Figure 2. NO reduction is the ratio of final NO concentration with propane addition, $[NO]_f$, to NO concentration without propane addition, $[NO]_i$. This is plotted as a function of second stage equivalence ratio, ϕ_2, for two values of the first stage equivalence ratio, ϕ_1. The reduction in NO achieves an optimum value at a second stage equivalence ratio of 0.4. The reduction of NO by two stage combustion is sensitive to the temperature of the second stage and to the equivalence ratio of both stages.

A major portion of our research effort has been devoted to the design and construction of a fluidized bed combustor. The most basic configuration of a fluidized bed combustor consists of a column into which a porous distributor plate has been fitted with bed material placed above the distributor plate. Fluidizing material, injected into the column below the plate, is forced to flow through the plate and bed. For relatively low flow rates, the viscous forces on the bed particle are overcome by gravitational forces. As the fluid velocity increases, a velocity termed the minimum fluidizing velocity is achieved whereby the two opposite forces on the bed particles are exactly balanced. At velocities in excess of the fluidization velocity, the bed expands and bed particles are free to move relative to one another.

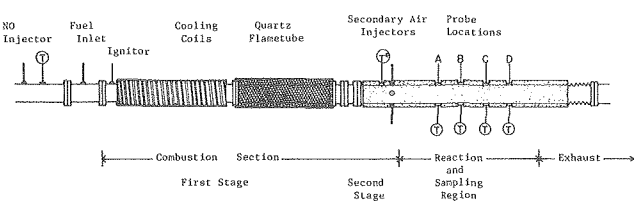

Fig. 1. Schematic diagram of combustion tunnel used for staging studies. (XBL 812-8257)

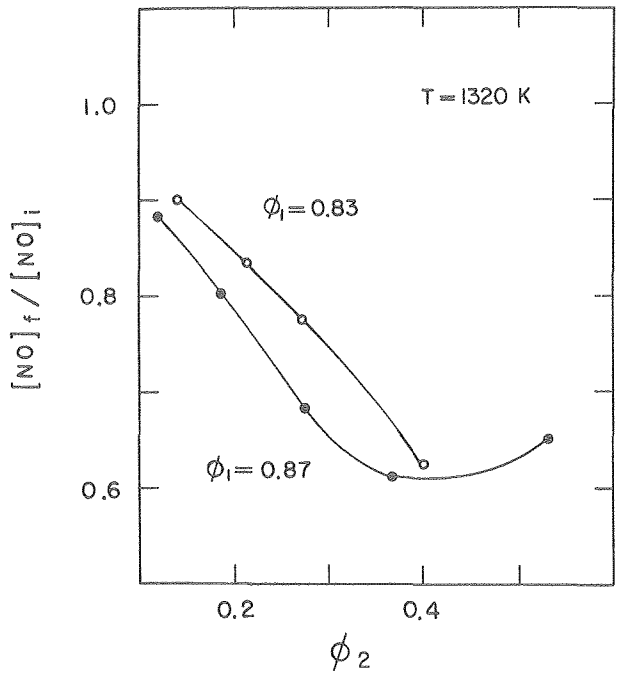

Fig. 2. Nitric oxide reduction as a function of second stage equivalence ratio ϕ_2, for first stage equivalence ratios 0.83 and 0.87. (XBL 812-8265)

Fluidized beds have characteristics which are extremely desirable in combustor design. Three of these (uniform bed temperature, low combustion temperature, and high heat transfer rates) are caused by vigorous mixing in the bed. These characteristics, which render fluidized beds remarkably insensitive to fuel properties, have great potential for reducing pollutant formation during combustion.

A multi-purpose experimental facility has been designed for the study of combustion staging in fluidized and spouted beds. Major design objectives for the facility are: (1) operation in a single, two, or three stage configuration; (2) operation in either a fluidized or spouted mode; (3) access for the insertion of temperature, pressure, and sampling probes; (4) optical access for visual observation and photographic studies, and (5) a simple two-dimensional flow geometry to ease data analysis. Assembly of the laboratory full-scale fluidized bed combustor has been initiated. A plexiglass model of one of the staged fluidized bed reaction sections was constructed and used to obtain cold flow characterization for the various fluidized modes; these are shown in Figure 3, where bed depth is plotted as a function of superficial velocity. The bed can be operated in packed, spouted, bubbling, and fluidized states.

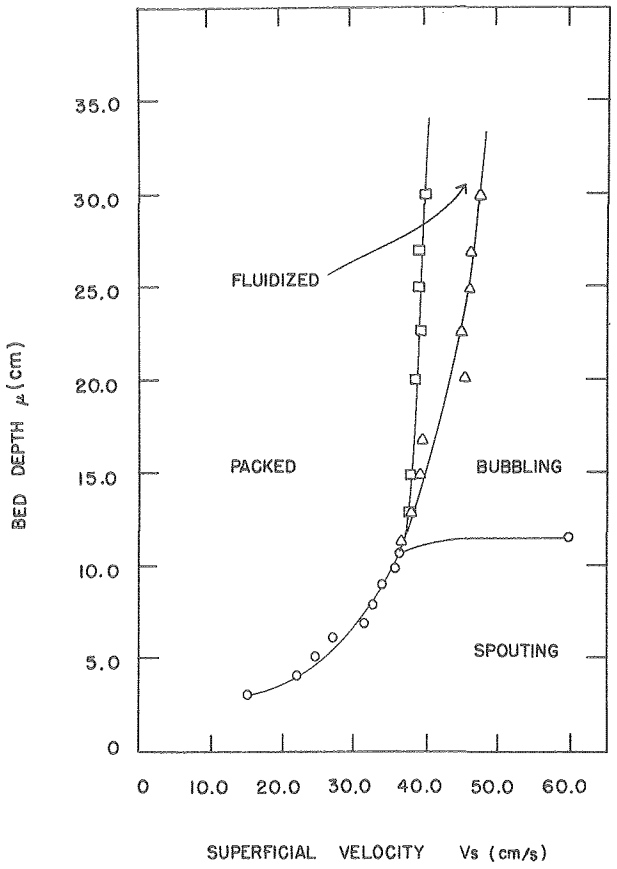

Fig. 3. Bed depth (cm) as a function of superficial velocity (cm/s) for cold flow characterization experiments. (XBL 812-8264)

PLANNED ACTIVITIES FOR FY 1981

Two types of staged combustion experiments (lean/lean and rich/lean) will be performed in the tunnel for two stages. The net equivalence ratio will be less than one (fuel lean). Propane will be mixed with variable amounts of simple nitrogen and sulfur compounds to simulate fuel nitrogen and fuel sulfur. The following compounds will be routinely measured: O_2, CO, NO, CO_2, SO_2, HCN, NH_3, and unburned hydrocarbons. Construction of the fluidized bed combustor will be finished, and characterization studies of cold and hot flow will be completed, using propane and propane doped fuels. Modelling studies of zero dimensional kinetics will be undertaken for nitric oxide reduction by staged combustion.

COLLISION DYNAMICS STUDIES OF HO_2 DISSOCIATION*

N. Brown and J. Miller†

INTRODUCTION

A detailed understanding of the kinetics of the hydrogen/oxygen flame system over a range of temperatures and densities typical of combustion systems is important. Reactions of the hydrogen/oxygen system play a unique role in combustion chemistry because they are sub-reactions in all hydrocarbon oxidation schemes. The specific chemistry of the radical species HO_2, which is formed as an intermediate during oxidation, is important in understanding: (1) ignition limits, (2) chain-branching, (3) heat release, and (4) radical shuffling mechanisms in combustion systems.

Our current research is concerned with investigating unimolecular reactions important to combustion processes. We are specifically interested in acquiring a better understanding of intramolecular energy transfer that dominates high pressure limit kinetics and is important in determining fall-off behavior. The existence of a realistic potential energy surface for the HO_2 molecule has provided us with a rather unique opportunity

* This work was supported by the Director of the Office of Energy Research, Office of Basic Energy Sciences, Chemical Sciences Division of the U.S. Department of Energy under Contract No. W-7405-ENG-48.

† Combustion Research Facility, Sandia National Laboratory, Livermore, CA

to investigate the statistical nature of intramolecular energy transfer in HO_2 for molecular energies in excess of the OH bond dissociation energy. This is important because advanced theories describe unimolecular reactions such as the RRKM[1] and adiabatic channel model[2] theories. These theories are based primarily on statistical approximations, and their success as a predictive tool depends greatly on the validity of these approximations.

ACCOMPLISHMENTS DURING FY 1980

Classical dynamics calculations were performed to investigate the dissociation reaction $HO_2 \rightarrow H + O_2$ at a fixed total energy in excess of that required to break the OH bond. The potential energy surface used to investigate HO_2 dissociation by intramolecular energy transfer is the analytical representation of the $^2A''$ state of HO_2 given by Melius and Blint[3] in their initial calculations. The $^2A''$ correlates with $H(^2S)$ and $O_2(^3\Sigma g)$ and is 17 kcal/mol below $HO_2(^2A')$. This surface has been used by Miller[4] to compute the thermal rate coefficient of the $H + O_2 \rightarrow OH + O$ reaction; the calculated results agree well with experiment results. Initial conditions for trajectory calculations were determined by Monte Carlo sampling the twelve dimensional phase space of the excited (above threshold) HO_2 molecule. A sampling technique used is similar to the Bunker[5] orthant sampling method and is suitable for averaging over sample sizes smaller than the number of orthants (2^{12}).

Dissociation times are defined as the time required to cross a 2.1 kcal/mol energy barrier in the exit channel separating $H + O_2$ from HO_2 on the surface. Fifty picoseconds are allocated for dissociation of each trajectory and those which did not dissociate in this time are deemed non-reactive. At the end of each reactive trajectory, the energy and angular momentum distributions in the products are determined. Final state attributes of several trajectories at a fixed total energy are histogrammed to verify whether the reaction was statistical.

Several interesting results emerge from our calculations. Figure 1 illustrates the distribution of reaction times for a sample of 355 trajectories at a total energy of 55 kcal/mol (approximately 10 kcal/mol above threshold). Also shown is a curve indicative of a random lifetime distribution:

$$\rho(t) = k\bar{e}^{kt}$$

where

$$\rho(t) = \frac{N}{N_0 \Delta t} \quad .$$

The rate coefficient and time are designated by k and t, respectively. The number of lifetimes, N, in each category is normalized by $N_0\Delta t$ where N_0 is the total number of trajectories and Δt is the lifetime interval width. Two features of Figure 1 indicate non-statistical, non-RRKM behavior. First,

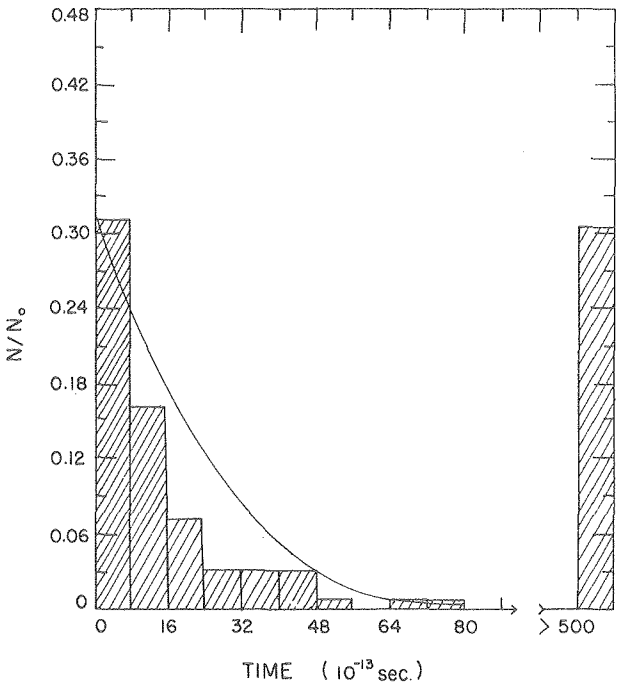

Fig. 1. Distribution of reaction times at a total energy of 55 kcal/mol. Solid curve represents random time distribution, histogram indicates calculated results. (XBL 814-9402)

only two-thirds of the trajectories are reactive in a fifty-picosecond time interval. Second, there are too few reactions at short reaction times and thus departures from the random distribution. This intrinsic non-RRKM behavior occurs when transitions between two or more vibrational states are slower than transitions leading to products. This is often the case when two vibrations have markedly different vibrational frequencies and is a manifestation of a light/heavy atom effect. It is possible that these long lived vibrational states may be characterized by quasi-periodic motion that persists over times of the order 10^{-10} sec and whose periodicity is energy dependent.

The distribution of final relative translational energy of the products H and O_2 is plotted in Figure 2 for reactive trajectories at 55 kcl/mol. This distribution is also markedly different from one predicted by an RRKM theory, which is a decaying exponential. Departures from non-RRKM translation energy distributions often indicate exit channel coupling effects. All reactive trajectories have final relative translational energies in excess of 2 kcal/mol; this indicates that energy requisite for surmounting the 2 kcal/mol energy barrier is released to the translational degrees of freedom and not to the internal energy of the O_2 molecule.

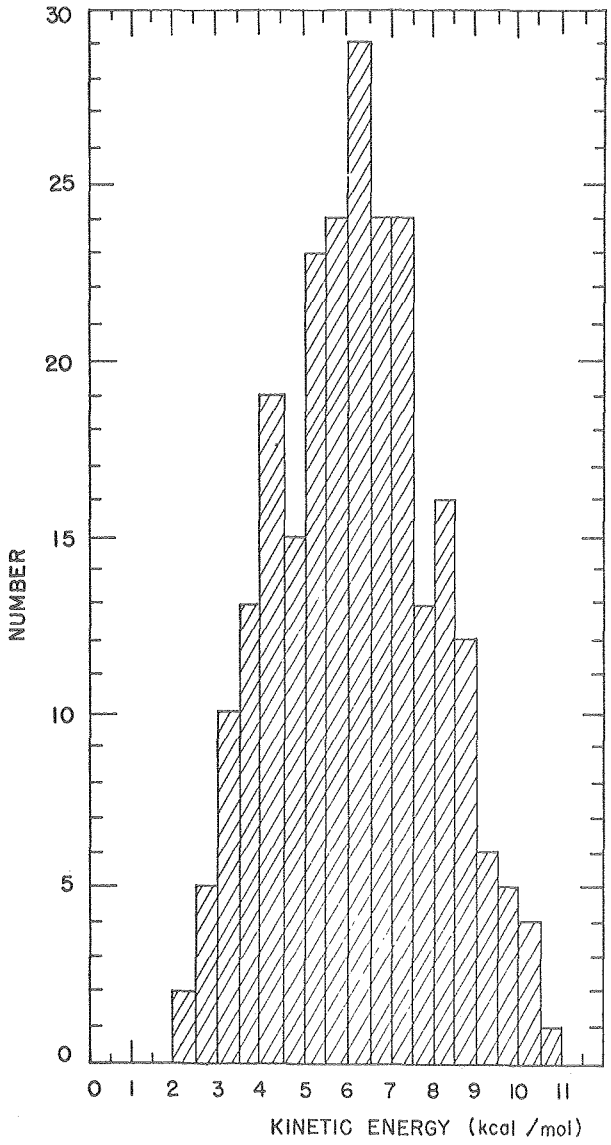

Fig. 2. Distribution of final relative translational energy for reactive trajectories at 55 kcal/mol. (XBL 812-8262)

PLANNED ACTIVITIES FOR FY 1981

Various techniques used to sample the 12 dimensional phase space will be compared, and criteria for determining whether or not sampling is representative will be developed. The effect of angular momentum on the reactivity of HO_2 will be investigated in detail. The fixed energy will be varied to provide additional reaction paths which, in turn, will be characterized. The most exciting aspect of our new work will also involve an in depth study of the non-reactive trajectories and a determination of their quasi-periodic nature. We will also study the dissociation of DO_2. Direct comparison of results obtained from dynamics studies will be compared with the results from statistical theories, whenever possible.

REFERENCES

1. R. A. Marcus, "Unimolecular Dissociations and Free Radical Recombination Reactions," J. Chem. Phys., vol. 20, p. 359 (1952).

2. M. Quack and J. Troe, "II Adiabatic Channel Model," Ber. Bunsenges. Phys. Chem., vol. 78, p. 240 (1974).

3. C. F. Melius and R. J. Blint, "Potential Energy Surface of the HO_2 Molecular System," Chem. Phys. Lett. vol. 64, p. 183 (1979).

4. J. A. Miller, "Collision Dynamics and the Thermal Rate Coefficient for the Reaction $H + O_2 \quad OH + O$," accepted for publication J. Chem. Phys. (1981).

5. D. L. Bunker, "Monte Carlo Calculations. IV Further Studies of Unimolecular Dissociation," J. Chem. Phys., vol. 40, p. 1946 (1964).

STATISTICAL THEORIES OF UNIMOLECULAR REACTIONS*

N. Brown and Abdel Hafez

INTRODUCTION

Recombination, dissociation, and isomerization reactions are classified as unimolecular reactions; these are important at various stages of combustion processes. The kinetics of unimolecular reactions are second order at low pressure where the reaction is rate-limited by the intermolecular transfer of energy. At the so-called high pressure limit, kinetics are first order and are limited by the rate of intramolecular energy transfer. The pressure associated with the high pressure limit is inversely related to molecular complexity and becomes higher as temperature increases. Kinetics in pressure regimes between the two limits, the so called fall-off regime, are influenced by both intermolecular and intramolecular energy transfer.

* This work was supported by the Director of the Office of Energy Research, Office of Basic Energy Sciences, Chemical Sciences Division of the U.S. Department of Energy under Contract No. W-7405-ENG-48.

There have been numerous attempts to describe unimolecular reactions theoretically; the most notable of these is the RRKM[1] theory. Although RRKM theory is often quite satisfactory for the prediction of rate coefficients for certain types of reactions, it is particularly poor for determining rate coefficients for simple bond fission reactions. Because these reactions lack a maximum in the electronic potential energy surface in the region of configuration space between reactants and products, it is difficult to describe the fixed activated complex which is implicitly assumed in RRKM theory. The RRKM theory is also deficient in its treatment of angular momentum effects. A more recent theory, the so-called phase space theory of Pechukas and Light [2], provides an improved treatment of angular momentum coupling but often overestimates rate coefficients. Reasons for the latter difficulty are not known although they are probably related to the loose transition state assumption.

Our current research is concerned with the improvement and application of statistical theories to the study of dissociation and recombination reactions of triatomic molecules: HO_2, H_2O, H_2S, SO_2, and $C\ell NO$. We compute the rate coefficients k (E,J) as a function of energy, E, and total angular momentum, J. This is appropriate for describing dissociation kinetics at the high pressure limit and is a major ingredient of the unimolecular rate coefficient in the intermediate fall-off regime. The number of states of the activated (energized above threshold) molecule and the density of states of the reactant molecule are determined and their ratio is proportional to k (E,J).

We are presently using the adiabatic channel model of Quack and Troe[3] and our own modification of the adiabatic channel theory. Adiabatic theories of reaction are characterized by the existence of so-called good quantum numbers which remain unchanged during the course of reaction. In triatomic dissociation reactions, the vibrational degree of freedom, termed the symmetric stretch, is considered adiabatic. Quantum numbers associated with the transition from bending vibration to hindered rotation to free rotation of the fragments which occurs during reaction are not good quantum numbers, and the degrees of freedom associated with these are termed diabatic. One degree of freedom is selected as a reaction co-ordinate, and the energy associated with the other degrees of freedom depends parametrically on the value of the reaction co-ordinate. We then compute the energy levels or channels of the energized molecules as a function of reaction co-ordinate and consistent with conservation constraints and adiabaticity. The energy terms in the energy channel expressions are of the following types: electronic, ro-vibrational, centrifugal energy, and zero point energy terms. The channel energies depend on the reaction coordinate through an exponential interpolation formula which connects reactant and product energy levels. A channel is open at a given energy, E, if the maximum energy of the channel is less than E. The number of open channels, W (E,J), is computed by determining channel maxima for those states of fixed, total-angular momenta and comparing the channel maxima with the total energy to determine whether the channels are open. The rate coefficient k (E,J) is computed according to

$$k(E,J) = \frac{W(E,J)}{h\,\rho(E,J)}$$

where h is Plancks constant and (E,J) is the density of states of the reactant molecule. The thermal rate coefficient k(T) is obtained by averaging k(E,J) over energy and angular momentum distributions.

ACCOMPLISHMENTS DURING FY 1980

We have successfully computed micro-canonical and canonical rate coefficients for reactions of triatomic molecules which dissociate into radical fragments. The rate coefficients, k(E,J), for the reaction $C\ell NO \rightarrow C\ell + NO$ is plotted in Figure 1 as a function of total energy above threshold $(E - V_o^\infty)$ for three values of total angular momentum. It is interesting to note that the dependence of the rate coefficient on total angular momentum changes with energy. An Arrhenius plot of a thermally averaged rate coefficient for the same reaction is shown in Figure 2. These results agree with those of Quack and Troe[3]. A new expression for the evaluation of channel energies has been determined which, hopefully, will better describe triatomic molecule dissociation reactions.

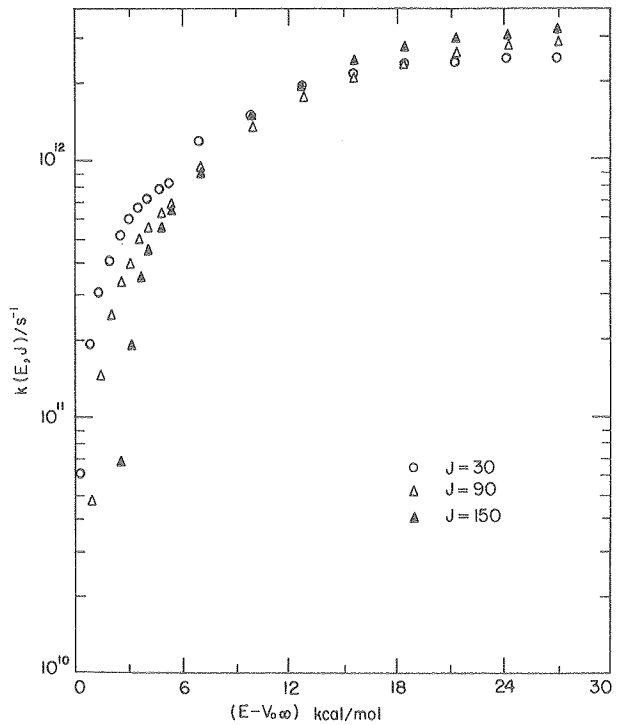

Fig. 1. Rate Coefficient k(E,J) in units of reciprocal seconds for the reaction $C_\ell NO \rightarrow C_\ell + NO$ as a function of energy above threshold, $(E - V_o)$ in (kcal/mol) for three values of total angular momentum. (XBL 812-8261)

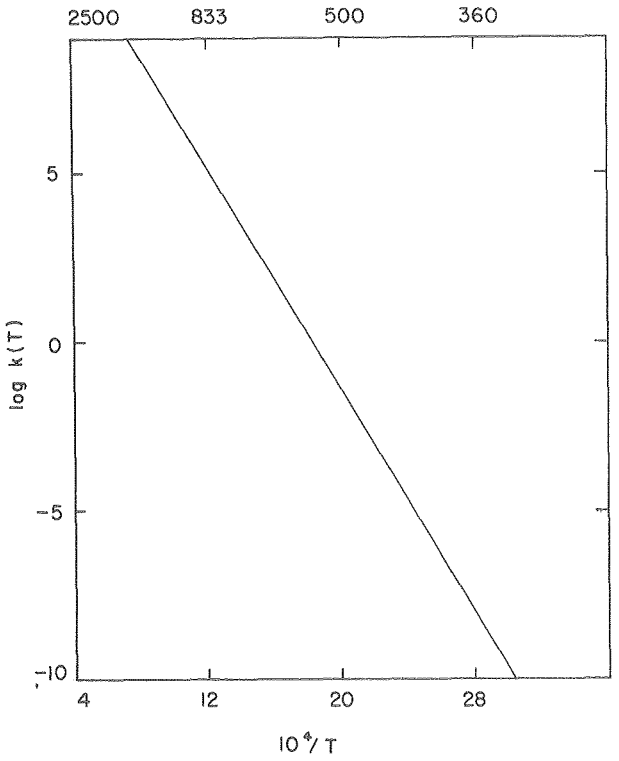

Fig. 2. Arrhenius plot of thermal rate coefficient (s^{-1}) for the reaction $C_\ell NO \rightarrow C_\ell + NO$. Temperature, T, is in degrees Kelvin. (XBL 812-8260)

PLANNED ACTIVITIES FOR FY 1981

Revised and regular adiabatic channel model calculations will be performed to determine microcanonical and canonical rate coefficients for HO_2, H_2O, H_2S, and SO_2. Sensitivity of computed results to energy level expressions and parameter dependence will be examined in detail. Adiabatic channel model results will be compared with experiment and with a minimum number of states calculation which properly describes angular momentum coupling.

REFERENCES

1. R. A. Marcus, "Unimolecular Dissociations and Free Radical Recombination Reactions," J. Chem. Phys., vol. 20, p. 359 (1952).

2. P. Pechukas and J. C. Light, "On Detailed Balancing and Statistical Theories of Chemical Kinetics," J. Chem. Phys., vol. 42, p. 3281 (1965).

3. M. Quack and J. Troe, "II Adiabatic Channel Model," Ber. Bunsenges. Phys. Chem., vol. 78, p. 240 (1974).

COMBUSTION DIAGNOSTICS BY TUNABLE ATOMIC LINE MOLECULAR SPECTROSCOPY*

E. Cuellar and N. Brown

INTRODUCTION

The characterization of emissions produced in the combustion of fossil fuels plays an important role in the utilization of energy resources. A detailed understanding of the chemistry of the combustion of sulfur containing fuels is of great importance, because sulfur, in the form of organic and inorganic compounds, can account for a significant proportion of the fuel mass. Corrosion in power plants due to sulfuric acid, atmospheric pollution by oxides of sulfur, and acid rain represent enormous problems which can seriously limit the full utilization of fossil fuels. Although much is known about the combustion chemistry of sulfur containing compounds[1], a basic mechanistic understanding of all of the decomposition and combustion reactions of even relatively simple molecules, such as H_2S or CS_2, is not yet available. Furthermore, the combustion kinetics of organic sulfur compounds, such as heterocyclic rings, is virtually unknown.

The principal sulfur containing product formed in the combustion of sulfur compounds is sulfur dioxide (SO_2). In addition to SO_2, numerous other sulfur containing species, e.g., SH, S_2, SO, H_2S are present in flames in significant proportions. Their identification and measurement is clearly of great importance if a detailed kinetic understanding of sulfur chemistry is to be obtained.

We present here results obtained with a new optical technique for measuring concentrations of species such as might be present in a combustion environment. This technique, called Tunable Atomic Line Molecular Spectroscopy (TALMS), is a line of sight, incoherent absorption technique which is highly sensitive and selective. TALMS is based on the Zeeman effect, which permits magnetic tuning of an atomic line into resonance with a molecular absorption[2]. Atomic absorption spectroscopy based on the Zeeman effect has been used in the analytical determination of numerous atomic species[3] and

* This research was supported by the Assistant Secretary for Environment, Office of Environmental Compliance and Overview, Environmental Safety and Engineering Division of the U.S. Department of Energy under Contract No. W-7405-ENG-48.

was recently extended to the detection of small molecules which exhibit sharp rotational electronic structure, e.g., NO (Reference 4) and SO_2 (Reference 5). We have applied this technique to the detection and measurement of S_2 formed in the equilibrium vapor of elemental sulfur and from the thermal decomposition of H_2S.

RESEARCH METHODS

A detailed description of the application of the Zeeman effect to atomic absorption spectroscopy has appeared elsewhere[6] and will be reviewed only briefly here. In the presence of an external magnetic field, atomic energy states which give rise to spectral lines may be split into new states by the Zeeman effect. Transitions between these new states produce an emission pattern with components which are not shifted (or shifted slightly) from the zero-field value ν_0 of the transition (the π components), and components which are shifted symmetrically to lower and higher energies about ν_0 (the $\sigma\pm$ components). Besides differing in frequency, the π and $\sigma\pm$ components also differ in their polarization.

The splitting of spectral lines produced by the magnetic field and the polarization of these lines form the basis for the detection of molecules by TALMS. By varying the strength of the magnetic field, one of the Zeeman components of the atomic emission line is tuned into exact coincidence with a sharp vibrational-rotational transition in the electronic absorption spectrum of the molecule to be detected; the other component is shifted off resonance. The matching component indicates the extent of absorption by the molecule of interest plus any background absorption due to other species present. The unmatched Zeeman component indicates background absorption only. A differential measurement of the absorption of the matched and unmatched components provides a quantitative measurement of the molecule to be detected.

Detection of S_2 and Magnetic Field Dependence

The electronic spectrum of S_2 has been extensively studied both in absorption and emission[7]. Particular attention has been devoted to the $B^3\Sigma_u^- \leftarrow X^3\Sigma_g^-$ system, extending from 2500 to 7000 Å and containing hundreds of bands which are resolved into rotational electronic transitions. The emission spectrum of chromium was selected as a good candidate for the detection of S_2, principally because there are several intense atomic lines around 3000 Å,[8] and the emission spectrum was easy to excite in a reasonably stable manner. Furthermore, SO_2, which is the principal sulfur-containing product in the combustion of sulfur compounds, absorbs in the region of 3000 Å; and selection of an atomic transition in this region would test the ability to detect S_2 in the presence of SO_2.

Several different cathode materials were used to produce the emission spectrum of chromium. Best results were obtained by spot welding several turns of nichrome tape (Tophet C, 16% Cr, 60% Ni, and 24% Fe) to the tip of the cathode, thus exciting the emission spectra of Ni, Cr, and Fe simultaneously. In this manner, relatively stable discharges could be obtained over a period of 2 to 4 hours.

Figure 1 shows the differential absorption signal obtained due to the matching of the atomic emission lines with individual S_2 molecular absorptions. The lower trace represents a section of the emission spectrum, while the upper trace, recorded simultaneously, is the output of the lock-in amplifier. The dotted lines between the two curves show that several atomic emission lines, each split into its own Zeeman pattern by the external magnetic field, give rise to differential absorption signals corresponding to a match of the Zeeman components of each line with a molecular absorption of S_2. Although any one of the matching lines (from Fe or Cr) could be used to detect S_2, we selected the Cr (I) line at 3018 Å because of its higher relative intensity. This Cr (I) emission line was assigned to the transition $^5D_3 \leftarrow {}^5F_4{}^0$ at 3017.57 Å (33,129.6 cm^{-1} vac.)[9].

The dependence of the differential absorption signal caused by S_2 on the strength of the external magnetic field is shown in Figure 2. As the field is increased from 2.5 kG, the signal decreases and passes through zero at about 8 kG. Increasing the field strength further results in differential absorption signals opposite in sign to those obtained at lower fields. This change in

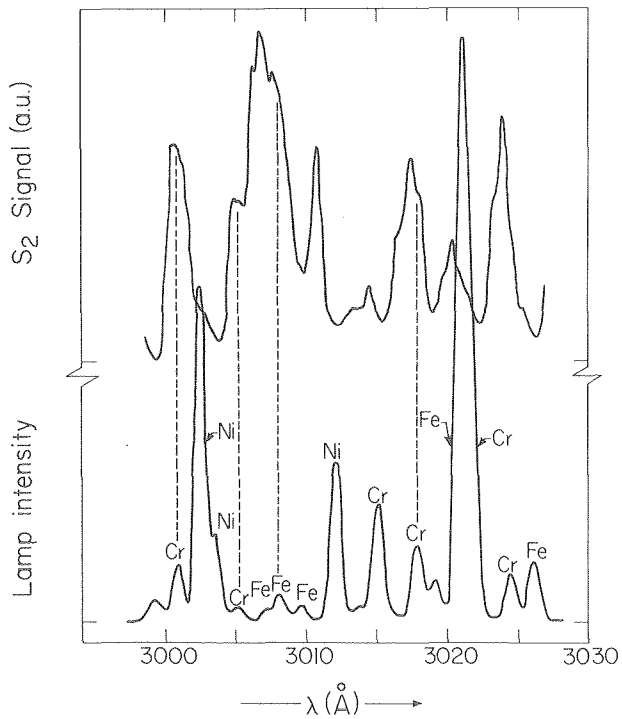

Fig. 1. The lower trace is a scan of the emission spectrum of nichrome tape. The upper trace monitors the differential absorption signals due to matching of the Zeeman split atomic emission lines with different molecular absorptions of S_2 (see text). Care must be taken to distinguish true differential absorption signals from excursions of the lock-in amplifier when the light intensity is near zero. (XBL-809-2034)

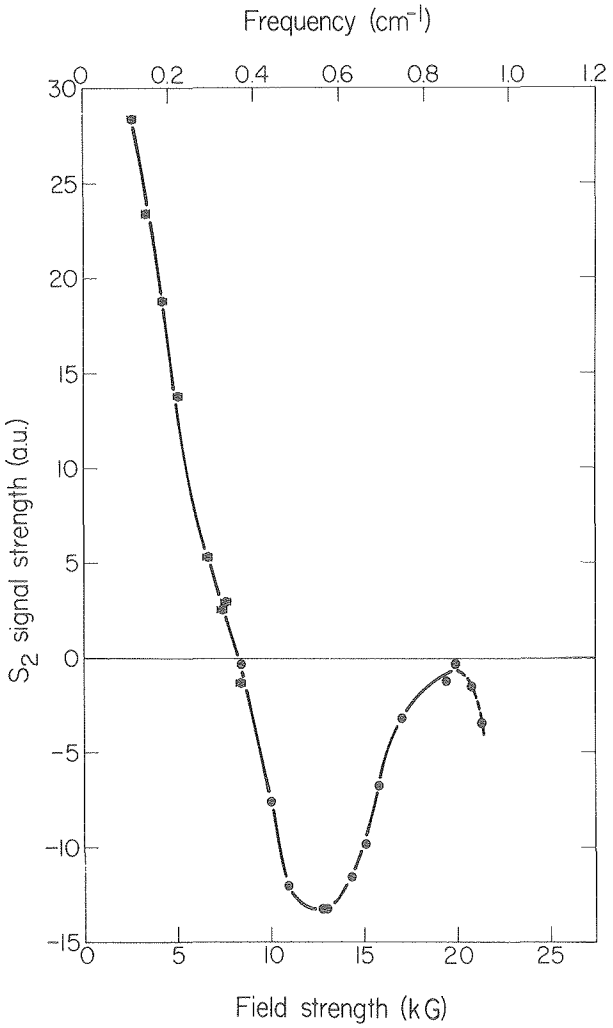

Fig. 2. Differential absorption signal due to S_2 as a function of the strength of the external magnetic field. $\Delta V_s = 0.0438\ cm^{-1}/kG$.
(XBL 809-2038)

polarity implies that at lower field strengths, one of the circularly polarized Zeeman components of the Cr (I) line, $\sigma+$ or $\sigma-$, is in resonance with a molecular absorption of S_2, while, at higher fields, this component falls off resonance while the other σ component tunes into a different absorption of S_2. Furthermore, the increasing positive signals observed at the lowest field strengths, where the separation between the + and - components is small, suggest that the center of the S_2 absorption which results in this positive signal is very close in frequency to the frequency of the zero field transition of the Cr (I) atomic line at 3018 Å. To interpret further the dependence of the S_2 absorption signals on the magnetic field strength, it is necessary to examine the spectroscopy of the $B^3\Sigma_u^- - X^3\Sigma_g^-$ system of S_2 in more detail.

Triplet Splitting of S_2

Frequencies for electronic transitions between individual rotational states within each vibrational manifold of S_2 were calculated using spectroscopic constants given by Huber and Herzberg [10]. As a first approximation, the finer details (due to electronic spin) of the rotational electronic structure of $^3\Sigma$ states were ignored and the rotational ladder within each vibrational level was considered to consist of single rotational levels for each value of K, the quantum number for total rotational levels for each value of K, the quantum number for total rotational angular momentum excluding spin. From this initial calculation, the frequency of the Cr (I) transition at 33,129.6 cm^{-1} could overlap with a low K line in the v', v" = 7, 2 band or with a high K (K ~ 60) line in the (4,0) band. Because S_2 is a homonuclear diatomic molecule and the nuclear spin of the ^{32}S nucleus is zero, even numbered K states are missing in the $X^3\Sigma_g^-$ state, and odd numbered K states are missing in the $B^3\Sigma_u^-$ state.

The rotation of the nuclei couples with the motions of the electrons (including spin) in a manner which increases the complexity of the energy level diagram of S_2. This coupling, plus the interaction between spins, splits each level given by the quantum number K into three levels, F_1, F_2, and F_3, with J = K + 1, K, and K - 1, respectively, where J is the total angular momentum, including spin.

The resulting energy level diagram for a value of K" = 13 in the (7,2) band of S_2 is shown in Figure 3. The transitions allowed for these

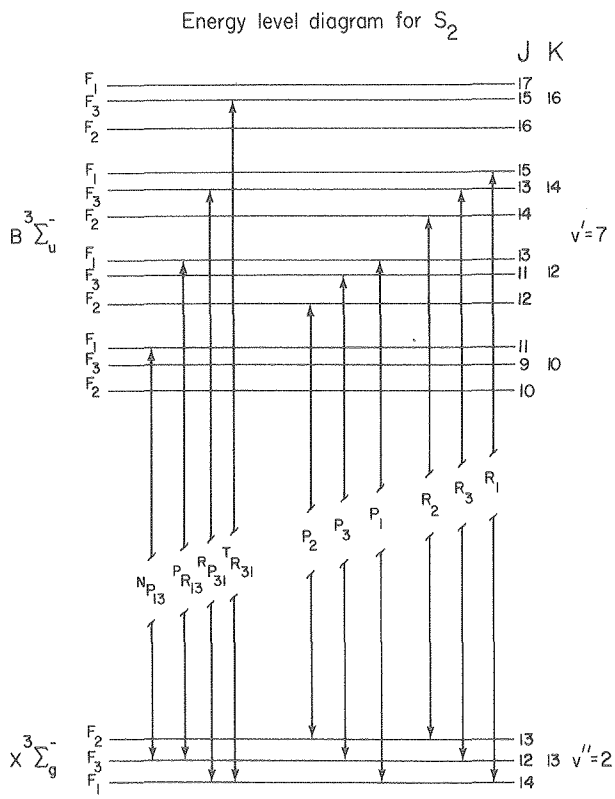

Fig. 3. Triplet splitting of the rotational levels of S_2. The v" = 2 level is normal while the v' = 7 level is inverted. The six main branches ($\Delta K = \Delta J$) and four satellite branches ($\Delta K \neq \Delta J$) are shown for K" = 13. The Cr (I) emission overlaps the $P_3(13)$ line. (XBL 809-2024)

triplet split states are also shown. There are six main branches which have $\Delta K = \Delta J$. These are indicated by $R_i(K)$ and $P_i(K)$, where i indexes the F_i levels involved. There are also four weaker satellite branches for which $\Delta K \neq \Delta J$: $^{T}R_{31}$, $^{N}P_{13}$, $^{R}P_{31}$, and $^{P}R_{13}$.

Frequencies for the six main branches and four satellite branches were calculated for K" = 1 to 60 using the expressions for F_1, F_2, and F_3.[11] Details of this calculation can be found in Reference [6]. The interpretation of the magnetic field dependence (Fig. 2) is shown in Figure 4. The Cr (I) atomic emission line at 3017.57Å (33,129.6 cm^{-1} vac.) is nearly resonant with the P_3 (13) branch of S_2, calculated at 33,129.7 cm^{-1}. At a field strength of 2 kG, the differential absorption is dominated by the σ- component, resulting in the large positive signal observed in Figure 2. As the field increases, the σ- and σ+ components spread apart and begin to overlap two other branches of S_2, R_2 (13) and R_1 (21), at 33,129.3 and 33,130.0 cm^{-1} respectively. At ~8 kG, the σ- and σ+ components overlap these two branches approximately equally, and, therefore, there is no differential absorption signal. Both of the σ components are attenuated equally by different S_2 absorptions. As the field increases to 13 kG, the σ- component moves off resonance from the

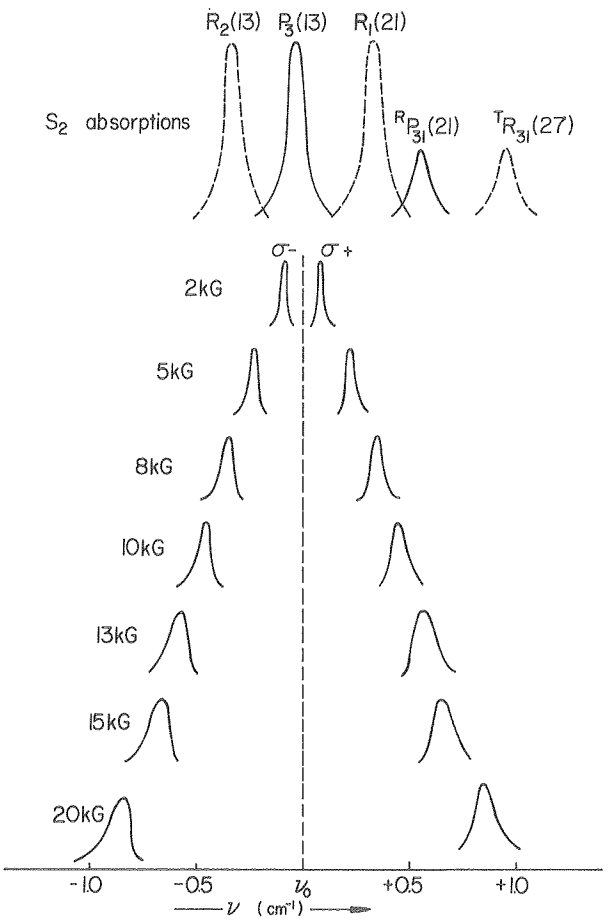

Fig. 4. Interpretation of the differential absorption signal for S_2 as a function of increasing magnetic field. (XBL 809-2031)

R_2(13) branch while σ+ overlaps the satellite branch $^{R}P_{31}$(21) at 33,130.2 cm^{-1}, resulting in a negative absorption signal. The roles of σ- and σ+, as monitors of S_2 and of background are reversed. Therefore, the polarity of the observed S_2 differential absorption signal is also reversed. As the field is increased further to 20 kG, the low frequency σ- component remains off resonance with any of the rotational branches of S_2 (the next branch is calculated to be $^{N}P_{13}$ (9) at 33,127.9 cm^{-1}), while σ+ begins to overlap T_{R31} (27) at 33,130 cm^{-1}. This overlap results again in an increasing negative differential absorption signal.

CONCLUSIONS

The technique of TALMS has been applied to the detection of the molecule S_2. An atomic transition in the emission spectrum of Cr (I) at 3017.57Å was found to be resonant with a rotational electronic absorption of S_2. By scanning the magnetic field from 0-20 kGauss, it is possible to map out several discrete absorptions of S_2 belonging to the v' = 7 ← v" = 2 band in the $B^3\Sigma_u^- \leftarrow X^3\Sigma_g^-$ system. These absorptions are identified as branches arising from the triplet splitting of the rotational states of S_2. It is interesting that rotational analyses for (v',v") bands of S_2 generally resolve only the main P and R branches, even with the use of high dispersion (~0.008 Å/mm) vacuum spectrographs. The weaker satellite branches have been detected only in fluorescence experiments, where a particular v', J' level is selected for excitation. It is remarkable that very high resolution, better than 6×10^4, is possible using the TALMS technique.

PLANNED ACTIVITIES FOR FY 1981

A major effort in FY81 will be devoted to the application of the TALMS technique to the measurement of NO and NO_2 in a CH_4 - air flat flame burner. The flat flame burner has been characterized, and the thermal NO produced can be compared with the results obtained using a chemiluminescent analyzer. A thorough study of the problem of third body quenching in the chemiluminescent analyzer will be conducted.

We will continue our efforts to develop techniques for detecting and measuring small molecules such as NH_3 and SO_2, in combustion environments. An atomic emission line in the spectrum of arsenic was recently found to be nearly resonant with an electronic transition of NH_3[12]. A weak differential absorption signal was observed using the TALMS technique, and further work will be required to improve the detection capability. SO_2 has been detected using a Zn line at 213.8 nm[5]. We propose to compare this optical technique with the conventional probe measurements of SO_2 using a commercial pulsed fluorescence SO_2 analyzer. A very significant problem associated with these SO_2 analyzers is the necessity to remove water from the sample gas and to make large corrections for third body quenching.

REFERENCES

1. C. F. Cullis and M. F. R. Mulcahy, "The Kinetics of Combustion of Gaseous Sulphur

Compounds," Comb. and Flame, vol. 18, p. 225 (1972).

2. H. Koizumi, T. Hadeishi, and R. D. McLaughlin, "Detection of Small Molecules by Magnetically Tuned Frequency-Modulated Atomic Line Sources," Appl. Phys. Lett. vol. 34, p. 382 (1979).

3. See for example T. Hadeishi and R. D. McLaughlin, "Hyperfine Zeeman Effect Atomic Absorption Spectrometry for Mercury," Science (London), vol. 174, p. 404 (1971); H. Koizumi and K. Yasuda, "An Application of the Zeeman Effect to Atomic Absorption Spectrometry: A New Method for Background Correction," Spectrochim. Acta Part B, vol. 31B, p. 237 (1976); H. Koizumi and K. Yasuda, "A Novel Method for Atomic Absorption Spectroscopy based on the Analyte Zeeman Effect," Spectrochim. Acta B, vol. 31, p. 523 (1977); Hideaki Koizumi and Kazuo Yasuda, "Determination of Lead, Cadmium, and Zinc Using the Zeeman Effect in Atomic Absorption Spectrometry," Anal. Chem., vol. 48, p. 1178 (1976).

4. H. Koizumi, T. Hadeishi, and R. D. McLaughlin, "A New Technique for the Determination of Isotopic Species Using Zeeman Scanning of an Atomic Line," Appl. Phys. Lett., vol. 34, p. 277 (1979); H. Koizumi, Tetsuo Hadeishi, and R. D. McLaughlin, "Nitric Oxide Determination by a Zeeman-Tuned Frequency-Modulated Atomic Line Source," Anal. Chem., vol. 52, p. 500 (1980).

5. H. Koizumi, T. Hadeishi, and R. D. McLaughlin, "Determination of SO_2 by a Zeeman Shifted Atomic Line," Anal. Chem. (to be published).

6. E. Cuellar, Detection of S_2 by Tunable Atomic Line Molecular Spectroscopy, Lawrence Berkeley Laboratory Report LBL-11323 (1980).

7. R. F. Barrow and R. P. du Parcq, in Elemental Sulfur (Beat Meyer, ed.), John Wiley and Sons, New York (1965), and references cited therein.

8. J. Reader and C. H. Corliss, "Line Spectra of the Elements," Handbook of Chemistry and Physics, 60th edition, CRC Press, Boca Raton, Florida (1979-1980).

9. J. Sugar and C. H. Corliss, "Energy Levels of Chromium, Cr I through Cr XXIV," J. Phys. Chem. Ref. Data, vol. 6, p. 317 (1977).

10. K. P. Huber and G. Herzberg, Molecular Spectra and Molecular Structure IV. Constants of Diatomic Molecules, Van Nostrand Reinhold Co., New York (1979).

11. G. Herzberg, Molecular Spectra and Molecular Structure I. Spectra of Diatomic Molecules, Van Nostrand Reinhold Co., New York (1950).

12. E. Cuellar, unpublished results.

SUBMICRON PARTICULATES FROM PULVERIZED COAL COMBUSTION*

J. Pennucci, R. Greif, G. Parsons, F. Robben, and P. Sherman

INTRODUCTION

During the combustion of pulverized coal, the bulk of the mineral matter is converted to fly ash. A fraction of the mineral matter may be vaporized and subsequently condense, either on existing particles or by forming new particles by the process of homogeneous nucleation.[1] The latter process results in a large number of particles in the size range 0.005 to 0.1 microns diameter; the size of typical ash particles is from 2-50 microns. Because of their small size, the submicron particles do not contribute substantially to the total mass of fly ash and may be overlooked. However, they can be a significant fraction of the total number of particles produced.

The submicron particles are most easily ingested into the lungs and may be a significant health hazard. Further, there is evidence that certain toxic trace elements are concentrated in the submicron particles, creating a greater health hazard than their prevalence would indicate.[2] Electrostatic precipitators and other cleanup devices effectively remove large particles, but their efficiency decreases for small particles, enabling them to pass into the atmosphere. Because the mineral matter in the coal is necessarily converted to ash during combustion, it is preferable that the ash particles be large to reduce their health hazard and to ease their removal from the stack gases.

This work consists of an experimental study of the effect of heat transfer and combustion parameters on the number and size distribution of particles in the submicron range and includes consideration of practical methods for control of the particles. The parameters studied are the flame temperature, cooling rate, and oxygen concentration in the fuel lean range. Peak temperatures have been varied from 1900 K to 2500 K. By changing the thermal resistance of the burner chimney

* This work was supported by the Assistant Secretary for Environment, Office of Environmental Research and Development, Environmental and Safety Engineering Division of the U.S. Department of Energy under Contract No. W-7405-ENG-48.

wall, cooling rates of 4000 KS^{-1} and 7000 KS^{-1} were obtained during the primary cooling period.

ACCOMPLISHMENTS DURING FY 1980

Details of the burner geometry are shown in Figure 1. The pulverized coal is entrained in a small amount of air and carried from the hopper to the burner. At the exit of the burner tube, the flame is stabilized by a ceramic flame holder. The chimney is used to prevent the burning mixture from mixing with the cool ambient air and to control the rate at which the flow is cooled. At the downstream end of the chimney, secondary air was injected to rapidly cool the products. The particle sampler was located 20 cm downstream of the chimney exit.

The particle sampler eliminates most of the large particles and collects the submicron particles on a carbon film surface. A transmission electron microscope is used to obtain photographs of the particles with resolution down to about 0.01 microns. The number of particles in various size ranges were manually determined.

The variation of the particle size and distribution with combustion and temperature is shown in Figure 2. The observed distributions appear to be a combination of two somewhat independent size ranges and physical effects. The number of particles in the range 0.01 to 0.02 microns was highly dependent on the cooling rate in the chimney, while particles in the range 0.02 to 0.05 microns do not appear to be dependent on the cooling rate. The effect of increasing peak temperature (higher methane concentration) was to increase the number of particles, particularly the larger ones, and shift the distribution toward the larger size ranges.

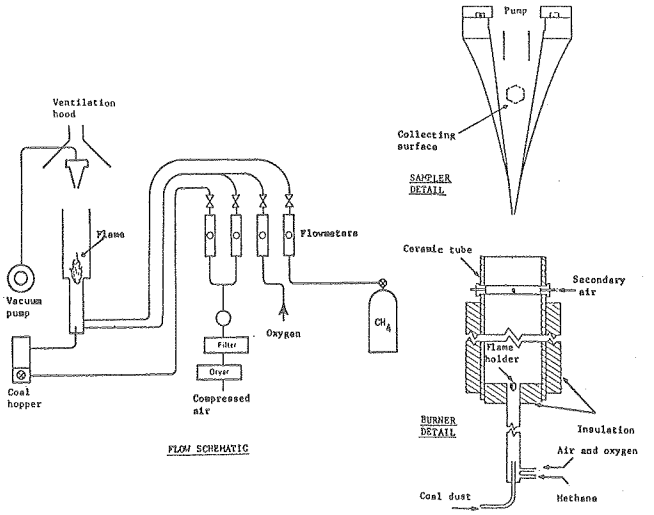

Fig. 1. Experimental apparatus. (XBL 811-7658)

Detailed presentation and results of these experiments is available.[3] In particular, the above mentioned result is believed to be caused by competition between homogeneous nucleation of new, small particles and condensation of the vapor on existing particles. With the higher cooling-rate uninsulated chimney, the temperature drops below the condensation point of the remaining vaporized ash; and most of the vapor condenses on pre-existing particles in the range 0.02 microns and larger. The rapid quench which accompanies the air injection at the end of the chimney does not result in any additional condensation. With the lower cooling rate, the vaporized ash remains in vapor form throughout the chimney and undergoes homogeneous nucleation during the rapid quench accompanying the air injection. In this case, we find a

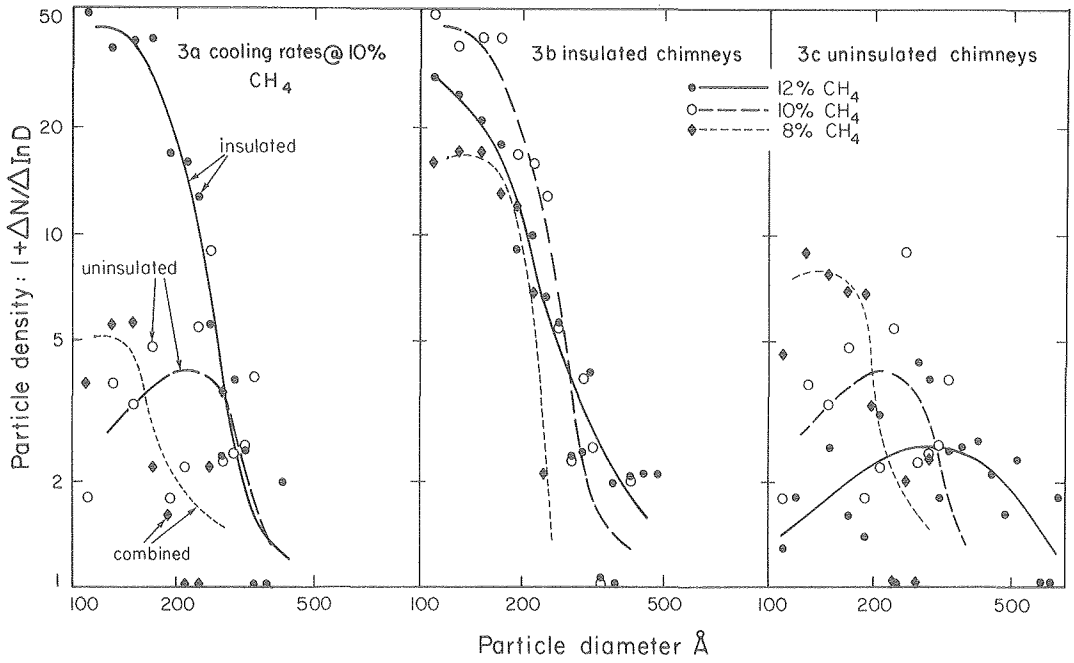

Fig. 2. Histograms of partial density versus diameter for different flame temperatures (percent methane) and cooling rates. (XBL 8012-2553)

much larger number of particles with sizes less than 0.02 microns.

Particles in the size range 0.02 to 0.05 microns may have been formed by homogeneous nucleation of another ash constituent, with a higher condensation temperature, immediately after the combustion region of the original coal particles. Their size would be dependent on the vapor characteristics and the rate of cooling, and a range 0.02 to 0.05 microns is reasonable.

These results are indications of the competition between homogeneous and heterogeneous nucleation which has been discussed in various models of pulverized coal fly-ash formation. The results indicate that it may be possible to control the smallest particles by varying the cooling rates in the post flame region.

PLANNED ACTIVITIES IN FY 1981

Investigation is planned to determine if certain toxic trace metals in coal are concentrated in the submicron portion of the fly-ash. For this purpose, an effective particle separator, probably of the impactor type, must be used to collect a sufficient sample of submicron particles to permit an x-ray fluorescence analysis of the atomic composition to be made. Initial measurements, using an LBL-developed sampler with two size fractions divided at 2 microns, has been successful. A suitable sampler will be obtained and similar studies on the particle size distribution will be conducted. Field test measurements on a large coal-fired steam boiler, using the same test equipment, would be very useful for comparison with the laboratory studies.

REFERENCES

1. R. C. Flagan and S. K. Friedlander, "Particle Formation in Pulverized Coal Combustion - A Review," Symposium on Aerosol Sciences, 82nd National Meeting, AICHE (1976).

2. R. D. Smith, "Laboratory Studies of Submicron Particles from Coal Combustion," Eighteenth Symposium (International) on Combustion, Waterloo, Canada (August 1980), to be published.

3. J. Pennucci, R. Greif, F. Robben and P. Sherman, Parametric Study of Submicron Particulates from Pulverized Coal Combustion, Lawrence Berkeley Laboratory Report LBL-12113 (January 1981).

SURFACE CATALYZED COMBUSTION*

R. Schefer and F. Robben

INTRODUCTION

Catalyzed combustion has been proposed as a method for promoting efficient burning of a variety of conventional and future alternative fuels with minimum pollutant formation. While preliminary tests have been quite promising, a number of aspects of catalyzed combustion are either not well understood or the necessary data are lacking. Necessary steps for the development of an optimum catalyst design will be: (1) to develop a greater understanding of the role of the catalyst in the combustion process, and (2) to determine high-temperature catalytic surface reaction mechanisms and reaction rates. It is the goal of the present study to provide some of the necessary understanding and data for catalytic combustor design.

Previous work has provided a detailed study of the combustion characteristics of lean H_2/air mixtures flowing over platinum catalytic and quartz (SiO_2) noncatalytic surfaces.[1] Regions were identified in which only surface reaction was present and others, at higher equivalence ratios and surface temperatures, in which both surface reaction and stable gas phase boundary layer combustion occurred simultaneously. Ignition temperatures were determined for surface reaction and gas phase reaction as a function of equivalence ratio, surface temperature, and surface reactivity (catalytic vs. noncatalytic). Surface energy release rates were measured and from these measurements models were developed for the high temperature surface oxidation of H_2.[2] Based on these models and known gas phase kinetic data for H_2/air reactions, a numerical computational scheme was developed for modeling H_2/air combustion in the presence of a catalytic surface and the effect of catalytic surface reactions on gas-phase combustion was investigated.[3]

ACCOMPLISHMENTS DURING FY 1980

During FY 1980, the combustion of lean C_3H_8/air and C_2H_6/air mixtures were studied extensively over platinum catalytic and quartz (SiO_2) noncatalytic surfaces, using Rayleigh scattering for boundary layer temperature measurements.[4] Based on the experimentally measured temperature profiles, gas phase ignition temperatures were determined over a range of operating conditions. Typical results for C_3H_8 are shown in Figure 1 where the surface temperature required for gas phase ignition is plotted as a function of equivalence ratio.

* This work was supported by Assistant Secretary for Conservation and Solar Energy, Office of Transportation Programs, Transportation Conservation Division of the U.S. Department of Energy under Contract No. W-7405-ENG-48.

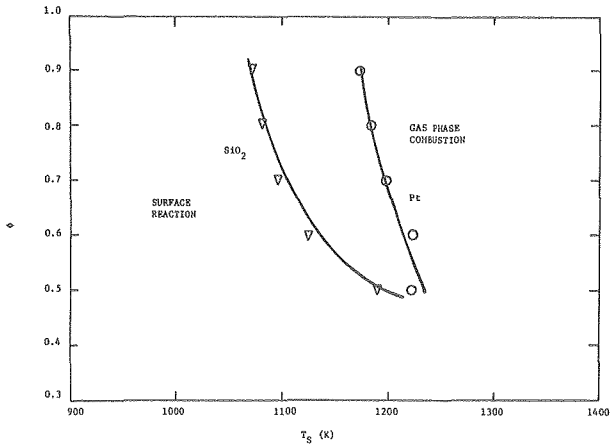

Fig. 1. Gas phase ignition temperatures for C_3H_8 combustion. U = 1.5 m/s. (XBL 812-8068)

It can be seen that, for both surfaces, the gas phase ignition temperature increases with decreasing equivalence ratio. At lower surface temperatures, i.e., higher equivalence ratios, the ignition temperature for the SiO_2 surface is approximately 100 K less than for the platinum. As the surface temperature increases, the ignition temperature for the SiO_2 surface approaches that of the platinum. This behavior is consistent with an increase in the catalytic activity of the quartz surface at higher temperatures. Numerical calculations for H_2/air mixtures flowing over a catalytic surface have shown that reactions at the surface, particularly surface oxidation of the fuel and radical recombination, result in a suppression of gas phase reactions in the boundary layer. Thus, at high equivalence ratios where a lower surface temperature is required for gas phase ignition, the noncatalytic nature of the quartz surface results in approximately a 100 K lower gas phase ignition temperature. At higher surface-ignition temperatures, where the catalytic activity of the quartz surface approaches that of the platinum, the gas phase ignition temperatures become comparable. Similar results were found using H_2/air and C_2H_6/air reactant mixtures.

Surface reaction ignition temperatures were also determined for C_3H_8/air and C_2H_6/air mixtures on a platinum surface. Ignition temperatures were found to be 470 K and 700 K, respectively, and were only a weak function of equivalence ratio. Based on experimentally measured values of surface heat release rates, surface oxidation rates were calculated for C_3H_8. This agreed well with a rate constant of the form $K_s = 1.1 \times 10^7 [C_3H_8]$ exp (-17000/RT) kg moles/m^2s. It was also found that, for temperatures less than approximately 670 K, CO is the primary oxidation product and that, for temperatures greater than 870 K, complete oxidation to CO_2 occurs.

A laser excited fluorescence technique was used to measure the OH radical concentration during combustion of H_2/air mixtures in the boundary layer of a heated platinum catalytic surface.[5] The technique consisted of exciting the OH molecule to the $A^2\Sigma$ ($v = 0$) excited state from a specific rotational level in the $X^2\Pi(v=0)$ ground state, using a narrow bandwidth pulse dye laser and monitoring the resulting band fluorescence at 32380 cm^{-1}. Relative OH concentration profiles were determined from the above fluorescence measurements, and absolute concentrations were determined from the integrated absorption spectra centered at 32380.99 cm^{-1}.

The measured OH concentration profiles using this technique are shown in Figure 2. These concentration profiles are highly nonequilibrium in character. For the hydrogen-air mixture (ϕ = 0.2) at the plate temperature of 1170 K, an OH concentration of 1.5×10^{13} (molecules/cc) would be expected at equilibrium. Near the leading edge (X = 5 mm), the peak OH concentration exceeds this equilibrium condition by a factor of 200, with a correspondingly high concentration near the plate surface. Proceeding further downstream, the peak OH concentration decreases slowly, being only a factor of two lower at X = 50 mm. than that closest to the leading edge. The decrease in the OH concentration nearest the plate surface with distance from the leading edge is the result of fuel depletion and recombination reactions. Near the free stream edge of the OH profile, the concentration drops very fast as the recombination reactions compete with the chain branching reactions of the H_2/O_2 system.

PLANNED ACTIVITIES FOR FY 1981

During FY 1981, work will continue on determining gas phase and surface ignition characteristics of conventional hydrocarbon and future alternative fuel/air mixtures flowing over a catalytic surface. From this additional data, it will be possible to determine with greater certainty the precise role of the catalyst and to determine both reaction mechanisms and kinetic constants for surface and gas-phase reactions. Catalyst operation under fuel-rich conditions will also be investigated, with emphasis on soot-formation characteristics in the presence of a high-temperature catalyst.

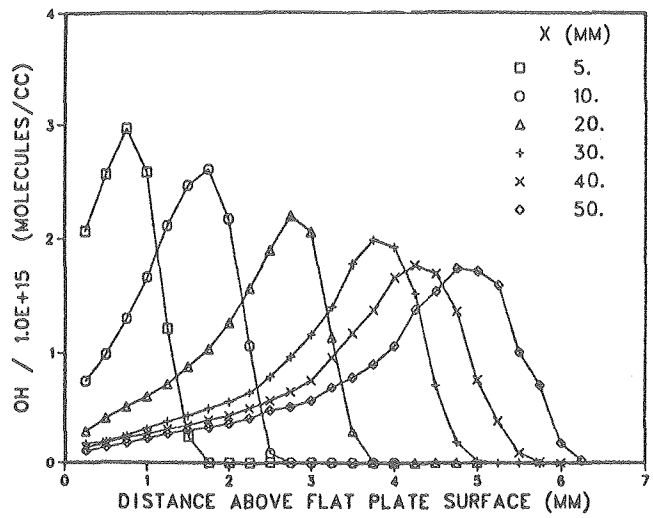

Fig. 2. OH concentration profiles for flow over a heated platinum surface. (XBL 812-8067)

REFERENCES

1. R. W. Schefer, F. Robben, and R. K. Cheng, "Catalyzed Combustion of H_2/Air Mixtures in a Flat Plate Boundary Layer: I. Experimental Results." Combustion and Flame, vol. 38, pp. 51-63 (1980).

2. R. W. Schefer, R. Cheng, F. Robben, and N. Brown, "Catalyzed Combustion of H_2/Air Mixtures on a Heated Platinum Plate." Western States Section/The Combustion Institute, Boulder, CO (1978).

3. R. W. Schefer, "Catalyzed Combustion of H_2/Air Mixtures in a Flat Plate Boundary Layer. II. Numerical Results." Combustion and Flame, to be published.

4. R. W. Schefer and F. Robben, "Catalyzed Combustion of Lean Fuel/Air Mixtures." Proceedings of the Fourth Workshop on Catalytic Combustion (1980).

5. R. J. Cattolica and R. W. Schefer, "Laser Fluorescence Measurements of the OH Concentration in Boundary Layer Combustion." Eastern States Section/The Combustion Institute, Princeton, NH (1980).

COMBUSTION FLUID MECHANICS

FLAME PROPAGATION IN GRID—INDUCED TURBULENCE*

R. Bill, Jr., R. K. Cheng, I. Namer, T. Ng, F. Robben, and L. Talbot

INTRODUCTION

The increase in flame propagation speed and volumetric heat release rate in a premixed turbulent flame relative to a laminar flame is important in designing combustion systems with optimum size and power characteristics. Although considerable attention has been given to the study of turbulent flame propagation, difficulties were encountered in obtaining measurements in the flame zone and, as a result, only gross properties of the flame have been studied. The effect of different turbulence scales and intensity on flame propagation was inferred by measuring the mean turbulent burning velocity. Questions concerning the effect of combustion on mean streamlines, turbulent kinetic energy, and turbulent length scales remained unanswered. Theoretical and numerical modes of turbulent flame propagation have focused attention on these problems. However, little data is available to guide theorists in their choice of proper models in turbulent combustion.

The objective of this program is to characterize the statistical nature of turbulent flame propagation by studying the change in scale and intensity of density and velocity fluctuations through the flame zone. This will be used to verify the assumptions of current and developing theoretical and numerical premixed flame models and to compare with the results of these models. The flame propagation is studied in low intensity grid-induced isotropic turbulence using laser diagnostics such as Rayleigh scattering and Laser Doppler Velocimetry (LDV).

ACCOMPLISHMENTS DURING FY 1980

Profiles were obtained of mean and fluctuation intensities of the streamwise component of velocity and the density through a v-shaped, premixed C_2H_4-air flame at several free stream velocities and mixture ratios.[1] The probability density function (pdf) and spectral density distribution at locations inside the flame were obtained. The experimental conditions covered flow velocities from 2.5 to 7.0 m/s and equivalence ratios from 0.55 to 0.75. Typical velocity root-mean-square (rms) fluctuation level was 4% of the free stream velocity.

Mean density and rms density fluctuation profiles through a flame are shown in Figure 1. The flame zone is characterized by the s-shaped mean density distribution. The density fluctuations shown are primarily due to the movement of the flame sheet across the measurement volume. The maximum intensity of 33% is typical for all results. The thickness of the flame zone at this location, 7.5 cm downstream from the grid, is about 4 mm and is found to increase at locations further downstream. Mean streamwise velocity profiles and corresponding rms fluctuation profiles are shown in Figures 2 and 3. The location of the flame zone at each axial location is indicated by the increase in velocity due to heat release. The locations of the peak rms velocity fluctuation are found to correlate well with the locations of peak density fluctuation. Behind the flame, the turbulence intensity decreased to approximately one-half of the level upstream of the flame. Thus, a substantial decrease in turbulent kinetic energy occurs. This is consistent with the result of numerical models.

* This work was supported by the U.S. Air Force Office of Scientific Research under Contract No. F44620-76-C-0083 through the Office of Research Service of the University of California, Berkeley. Additional facility and equipment support was provided by the Director of the Office of Energy Research, Office of Basic Energy Sciences, Chemical Sciences Division of the U.S. Department of Energy under Contract No. W-7405-ENG-48.

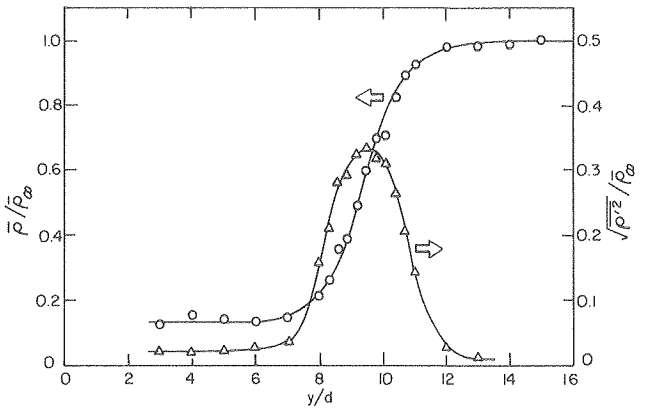

Fig. 1. Mean and rms intensity profiles of density. U_∞ = 6.84 m/s, ϕ = 0.75, d = 1.0 mm, x = 7-5 cm.
(XBL 809-5938)

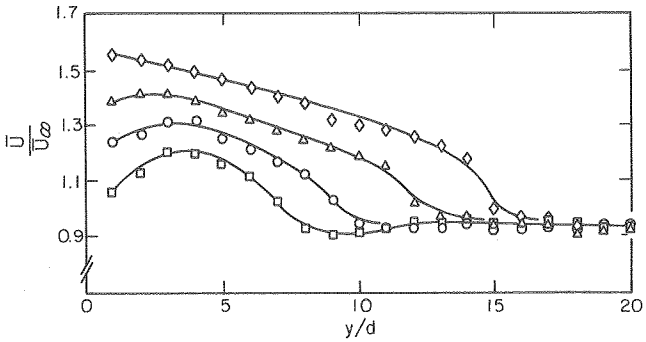

Fig. 2. Mean velocity profiles through a flame. U = 6.84 m/s; ϕ = 0.75; d = 1.0 mm, □; x = 7.0 cm, O; x = 7-5 cm, △; x = 8.0 cm, ◇; x = 8.5 cm.
(XBL 802-368)

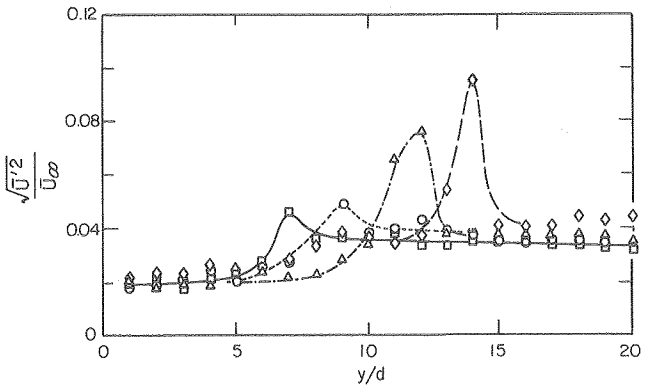

Fig. 3. Turbulence intensity profiles conditions. U_∞ = 6.84 m/s; ϕ = 0.75, d = 1.0 mm, □; x = 7.0 cm, O; x = 7-5 cm, △; x = 8.0 cm, ◇; x = 8.5 cm.
(XBL 802-370)

To verify the assumption of the Bray-Moss-Libby model[2] that the gas consists simply of burnt products and unburnt reactants, pdf's of density were computed at locations[3] inside the flame zone (Fig. 4). These pdf's show that the intermediate state between burnt product and unburnt reactants constitutes as much as 30% of the gas in the flame. A comparison of statistics for fluctuation intensity and skewness with results predicted by this model indicate that the model overpredicts these statistical moments.[3]

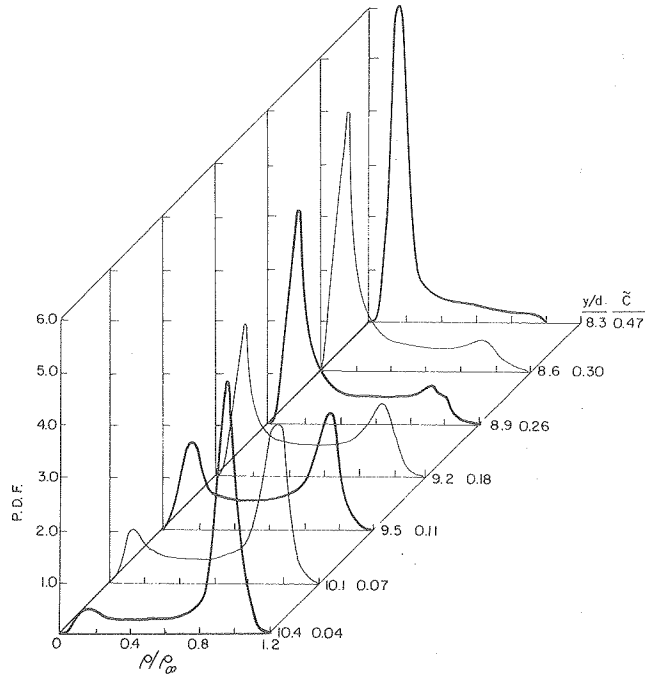

Fig. 4. Evolution of pdf's through a flame. U_∞ = 6.84 m/s, ϕ = 0.75, x = 7-5 cm.
(XBL 807-5565)

PLANNED ACTIVITIES FOR FY 1981

Diagnostic techniques for measuring spatial correlation of density fluctuation will be developed. This will involve obtaining Rayleigh scattering from two measurement points. These results will provide insight into the scale and intensity of the flame front movement to properly interpret the Reynolds stress and other velocity measurements inside the flame.

REFERENCES

1. R. G. Bill, Jr., I. Namer, L. Talbot, R. K. Cheng, F. Robben, "Flame Propagation in Grid Induced Turbulence," to appear in Combustion and Flame, 1981.

2. K. N. C. Bray and P. Libby, "Interaction Effects in Turbulent Premixed Flames," Phys. of Fluids, vol. 19, p. 1687 (1976).

3. R. G. Bill, Jr., I. Namer, L. Talbot, and F. Robben, "Density Fluctuations in Turbulent Flames" submitted for publication in Combustion and Flame, to be published.

COMBUSTION IN A TURBULENT BOUNDARY LAYER*

R. K. Cheng, R. Bill, Jr., T. Ng, F. Robben and L. Talbot

INTRODUCTION

Although turbulent combustion occurs in most practical combustor configurations, the interaction between fluid mechanical turbulence and combustion heat release is not well understood due, in part, to the lack of sufficient experimental data on turbulence in combustion environments to develop an analytical description of the process. With the advancement of laser diagnostics in recent years, it is now possible to obtain time- and space-resolved measurements of turbulent parameters in combustion. The objective of this program is to study premixed turbulent combustion in a well-defined configuration, in this case a heated turbulent boundary layer. This study will contribute to the experimental data base necessary for development of theoretical and phenomenological models of turbulent combustion.

Using a heated wall turbulent boundary layer to study combustion has some advantages over more conventional combustion systems, such as flames. By adjusting wall temperature and mixture ratios, combustion heat release can take place throughout the boundary layer, permitting an alternate means for studying the combustion-turbulence interaction. Characteristic features of H_2-air combustion in a heated boundary layer near transition have been studied in a small (2.5 cm square) channel.[1] This facility was built as the prototype of a larger (10 cm square) wind tunnel for the study of combustion in a fully-developed turbulent boundary layer.

ACCOMPLISHMENTS DURING FY 1980

Experiments in the 10 cm square channel have been carried out in the heated turbulent boundary with and without H_2-air combustion. This wind tunnel is driven by a centrifugal fan and is mounted on a 3-axis stepping-motor-controlled traverse mechanism. In the present experiment, the boundary layer develops in an unheated section 0.5 m in length before entering the heated bottom wall section 0.25 m in length. The heated wall consists of nine electrically heated Kanthal strips stretched over ceramic blocks.

The heated wall flow without combustion was studied in detail by the use of Rayleigh scattering and Laser Doppler Velocimetry (LDV). The diagnostics are interfaced with a computer-controlled data acquisition system based on a PDP 11/10 computer. Using a CDC 7600 computer, data analysis was made by transferring the raw data on magnetic tape. Density, velocity and Reynolds stress profiles as well as probability density functions and spectral density distributions were obtained at each measurement point.[2]

Typical experimental conditions were free stream velocity of 20 m/s and wall temperature of 1000 K. In the unheated case, both the velocity and Reynolds stress profiles were in reasonably good agreement with hot-wire data reported in the literature. In the heated wall case, the temperature profiles obtained from density measurements followed a power law. However, no similarity was found between the mean temperature and velocity profiles, in contrast to the similarity found in a slightly heated wall ($\Delta T \approx 20$ K) turbulent boundary layer.[3] Shown in Figure 1 are mean and fluctuation profiles obtained at various axial stations along the heated wall section. In all, the velocity fluctuations were found to be increased slightly by wall heating. Comparison of the Reynolds stress profiles obtained with and without wall heating (Fig. 2) demonstrated that the Reynolds stress near the wall was reduced by heat transfer from the wall.

The experiments involving H_2-air combustion in the boundary layer were studied using high-speed laser schlieren cinematography to determine the conditions at which various modes of boundary layer combustion would occur. These movies have shown that the turbulence structures were not altered by lean H_2-air combustion and that large scale coherent turbulent structures were not apparent in this turbulent boundary layer.

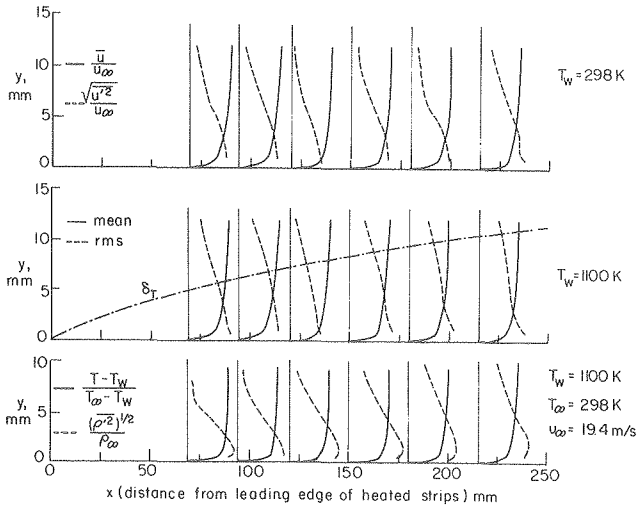

Fig. 1. Comparison of mean and fluctuation profiles of velocity and density profiles in heated and non-heated turbulent boundary layer. S_T = thermal boundary layer thickness based on ρ/ρ_∞ = .99. (XBL 8011-6364)

* This work was supported by the Director of the Energy Research, Office of Basic Energy Sciences, Chemical Sciences Division of the U.S. Department of Energy under Contract No. W-7405-ENG-48.

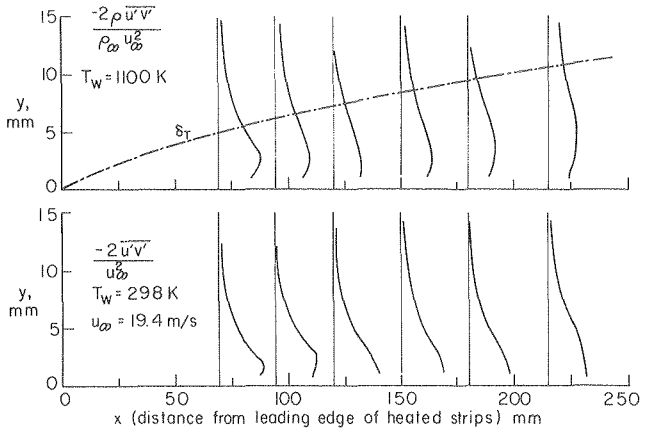

Fig. 2. Comparison of Reynolds stress

$$(\overline{-2u'v'}/u_\infty 2)\ (\rho/\rho_\infty)$$

profiles in heated and non-heated turbulent boundary layers. (XBL 8011-6363)

PLANNED ACTIVITIES FOR FY 1981

Completion of the data analysis will provide a comprehensive description of the turbulent flow field in the heated boundary layer. Detailed measurements of C_2H_4-air combustion in the heated boundary layer will be made. Comparison of these data will make possible the study of the effect of combustion on the turbulence parameters.

In addition to measurements using existing diagnostic tools, more advanced laser diagnostic techniques will also be developed to obtain cross-correlations between fluctuation parameters. These will include combined Rayleigh and LDV to measure the cross-correlation between velocity and density and a two component LDV system to measure instantaneous Reynolds stress. These quantities are important for the study of turbulent kinetic energy exchange in combustion regions.

REFERENCES

1. R. K. Cheng, R. G. Bill, Jr., and F. Robben, "Experimental Study of Combustion in a Turbulent Boundary Layer" to appear in 18th (International) Symposium on Combustion, The Combustion Institute (1980).

2. R. K. Cheng and T. T. Ng, "Measurement of Density and Reynolds Stress in a Heated Wall Turbulent Boundary Layer," Bulletin of the American Physical Society, vol. 25, no. 9, p. 1019 (1980).

3. W. C. Reynolds, W. M. Kays and S. J. Kline "Heat Transfer in the Turbulent Incompressible Boundary Layer, I - Constant Wall Temperature," U.S. National Aeronautics and Space Administration Report, NASA Memorandum 12-1-58W, 1958.

NUMERICAL MODELING OF TURBULENT COMBUSTION*

A. Ghoniem, A. Chorin, and A. Oppenheim

INTRODUCTION

Combustors in all practical power plants are operated under turbulent flow conditions. Good understanding of the mechanism of such flows is important in developing proper means for the control of the combustion process, an essential requirement for the attainment of clean exhaust and efficient performance. Of particular significance is the numerical modeling technique we developed, as described in the 1979 Annual Report (p. 6-38ff), based on the random vortex method (RVM) due to Chorin.[1]

This method was designed to develop a satisfactory approximation to the solution of the equations describing the flow without the use of finite differencing, a conventional technique that inherently obscures the mechanism of turbulence. In RVM, essential features of the flow field are mimicked by the action of vortex elements modeling the essential ingredients of turbulence, the elementary eddies. Their random walks express the effects of diffusion, while compliance with the tangential boundary condition at the walls is assured by creation of vorticity in the proper amount. A potential flow solution is used at the same time, using the principle of fractional steps to guarantee that the normal boundary condition is satisfied.

The RVM keeps track of the position and strength of all the vortex elements constituting the flow field and is thus essentially grid-less. It is therefore devoid of the smoothing, intrinsic to the finite difference technique, and unaffected by the numerical diffusion it introduces. Above all, RVM does not involve any averaging whatsoever. On the contrary, instead of damping the disturbances, it actually introduces a certain amount of randomness, or numerical noise, simulating the mechanism of local perturbations in a way similar to the one which occurs in real flow.

* This work was supported by the Director of the Office of Energy Research, Office of Basic Energy Sciences, Division of Chemical Sciences of the U.S. Department of Energy under Contract No. W-7405-ENG-48, and by the U.S. National Aeronautics and Space Administration under Grant No. NSG 3227 through the Engineering Office of Research Service, University at California, Berkeley.

ACCOMPLISHMENTS DURING FY 1980

In 1979, we obtained results modeling the turbulent flow in a two-dimensional combustion tunnel with the flame stabilized behind a rear-facing step (1979 Annual Report, p. 6-38ff). We have now included the exothermic effects of combustion adding a new algorithm for handling flame propagation to the vortex dynamics. The structure of the full computational scheme describing the two algorithms and their interrelationship is shown in Figure 1. It should be noted that, whereas vortex dynamics refers to a solenoidal field associated with vorticity generation, flame propagation involves an irrotational field, the exothermic effects of combustion being expressed in terms of potential volumetric sources. Thus, according to our model, the only way combustion can affect turbulence is by augmenting the velocity vector field which, in turn, gives rise to new vortex elements caused by the no-slip condition at the walls, as indicated at the left upper corner of Figure 1.

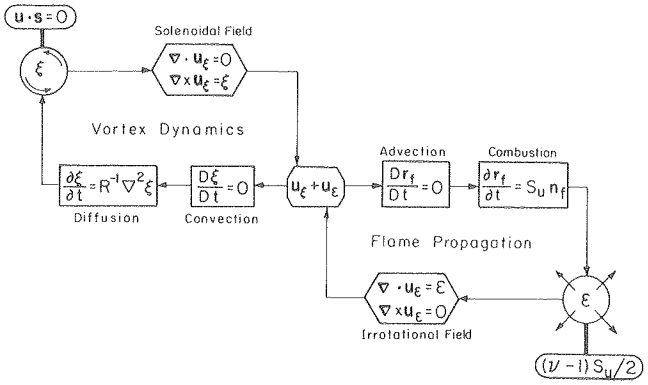

Fig. 1. Structure of the computational scheme. (CBB 802-2190)

Our studies were reviewed at the 18th Combustion Symposium[2] and described in an LBL Report.[3] Pertinent results of these studies are presented in Figure 2 which illustrates two sequential series

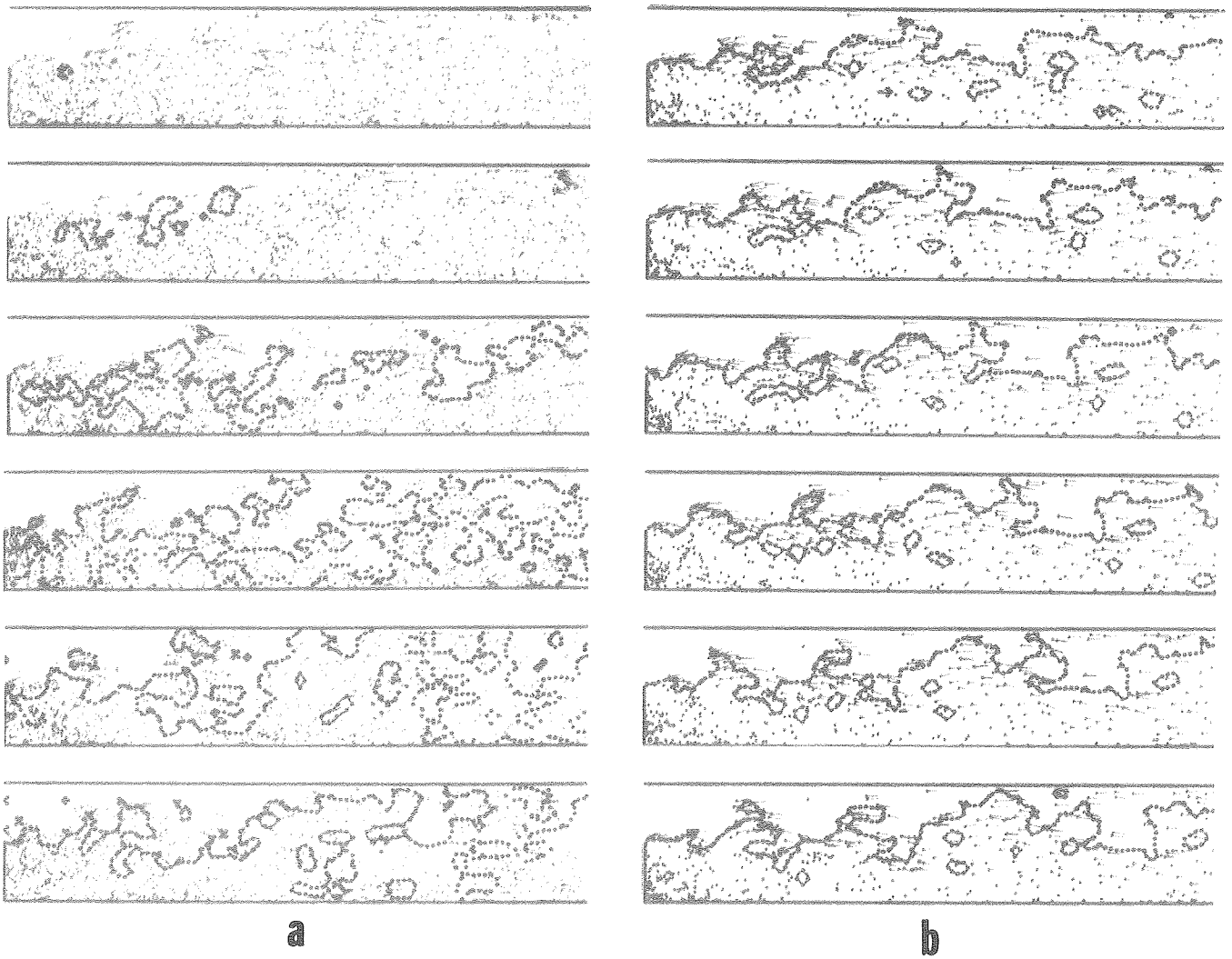

Fig. 2. Sequential series of computer plots displaying vortex velocity fields and flame fronts in turbulent combustion behind a step at Reynolds number of 10^4, while the ratio of the normal flame velocity to the flow velocity at inlet is 0.02. (a) Ignition in a fully developed turbulent flow at a point situated at the level of the step one step height downstream. (b) Fully established turbulent combustion in the flow field behind the step. (CBB 802-2190)

of computer outputs depicting the variation of the velocity fields and flame fronts. The series are expressed in terms of velocity vectors represented, as usual, by line segments providing information on their magnitude and direction. However, instead of being furnished with conventional arrowheads, the vectors are attached at their origin to small circles denoting the locations of the vortex elements to which they pertain. The flame front is depicted by closely spaced series of dots forming distinct contours.

The sequence in Figure 2a depicts the process of ignition in a turbulent flow field which has been already established in the combustion tunnel behind a rear-facing step. The combustible medium to which it pertains is a lean propane/air mixture, whose normal flame speed is 12 cm/sec, flowing at a velocity of 6 m/sec (corresponding to the Reynolds Number of 10^4). The sequence at the left bottom corner of Figure 2b displays the combustion field following ignition initiated at the moment when the medium was set in motion. In both cases, the effects of the turbulent flow field are quite remarkable if one realizes that it was capable of stabilizing the combustion process under conditions where the normal burning velocity was only 2% of the average velocity of flow. The relative ease with which a continuous flame front was established in the latter case demonstrates the importance of proper timing and location of the ignition source.

PLANNED ACTIVITIES FOR FY 1981

Using the method we developed, it is our intention now to examine the properties of turbulent flow fields under the geometrical conditions modeling the essential features of bluff body flame holders with and without combustion. Of particular interest in this respect are: the mean velocity profiles, the Reynolds stresses, and the pressure profiles--quantities which can be compared with available experimental data.[4]

We also intend to apply our numerical modeling analysis to the study of the unstable behavior of flow behind a step. Of special significance here is the effect of enriching the fuel/air mixture, leading to various modes of instabilities that have been identified recently in an experimental program of research completed.[5]

The RVM will be applied, moreover, to the analysis of combustion in jets, the major subject of our studies on ignition described elsewhere in this Annual Report.[6] This should be particularly helpful in assessing the effects of distributed ignition centers that can be achieved by the use of active radicals.

Finally we will be working on the development of novel random element methods, using RVM as the basis, to model heat transfer processes, so that their effects in combustion systems could be included.

REFERENCES

1. A. J. Chorin, "Numerical Studies of Slightly Viscous Flow," J. Fluid Mech., vol. 57, pp. 785-796 (1973).

2. A. F. Ghoniem, A. J. Chorin, and A. K. Oppenheim, "Numerical Modeling of Turbulent Combustion in Premixed Gases," Eighteenth Symposium (International) on Combustion, The Combustion Institute, in press (1981).

3. A. F. Ghoniem, A. J. Chorin, and A. K. Oppenheim, "Numerical Modeling of Turbulent Flow in a Combustion Tunnel," Lawrence Berkeley Laboratory, LBL-11520 (1980).

4. R. W. Pitz and J. W. Daily, "Experimental Study of Combustion in a Turbulent Free Shear Layer Formed at a Rearward Facing Step," AIAA 19th Aerospace Sciences Meeting, St. Louis, Mo. (January 1981).

5. J. O. Keller, L. Vaneveld, D. Korschelt, G. L. Hubbard, A. F. Ghoniem, J. W. Daily, and A. K. Oppenheim, "Mechanism of Instabilities in Turbulent Combustion Leading to Flashback," AIAA 19th Aerospace Sciences Meeting, St. Louis, Mo. (January 1981).

6. A. Oppenheim, F. Hurlbut, F. Robben, R. Peterson, P. Coico, and H. Stewart, "Ignition Studies," Lawrence Berkeley Laboratory, Energy and Environment Division Annual Report FY-1980, LBL-11650.

VORTEX INTERACTION WITH A PREMIXED LAMINAR FLAME*

I. Namer,† R. Bill, Jr.,†† F. Robben, and L. Talbot

INTRODUCTION

As part of a research program on premixed turbulent flame propagation, the interaction of an otherwise laminar flame front with the vortices produced in the wake of a single rod (the so-called Kármán vortex street) has been studied. The goal of this work is to provide greater insight into turbulent flame propagation under conditions where the wrinkled laminar flame model should apply. Measurements have been made of velocity, using laser Doppler anemometry, and density, using Rayleigh scattering; and mean turbulence levels, probability density functions, and power spectra have been obtained. In addition, the regularity of the vortex street has allowed the use of phase-locked signal averaging to obtain the instantaneous velocity fields from a time averaged ensemble of reasonably repeatable vortices. A complete description of this experiment and the results obtained has been prepared[1] and a previous report on some preliminary work is also available.[2]

ACCOMPLISHMENTS DURING FY 1980

Measurements were made in a small open jet wind tunnel which produced a 50mm diameter jet of premixed ethylene and air. A sheet flame was stabilized on a small rod, and a larger upstream rod produced the vortex street, shown schematically in Figure 1. The fuel-air jet was surrounded coaxially by an air jet of the same velocity, which served to reduce the turbulence level at the fuel jet boundary and thus to minimize the flowfield and flame front fluctuations originating in the jet boundary region of the flame.

A one-watt argon-ion laser was the source for both the LDA and Rayleigh measurements. The Laser Doppler Anemometry (LDA) was a dual beam, real fringe type, using a Thermal Systems, Inc. (TSI) tracker to produce a voltage proportional to the velocity of each validated particle. The intensity of the Rayleigh scattered light was measured at right angles to the laser beam using about f/2.4 optics, a filter, and an RCA type 931A photomultiplier. The results were recorded by a PDP-11 computer and stored on magnetic tape for final data reduction on a large (CDC 7600) computer.

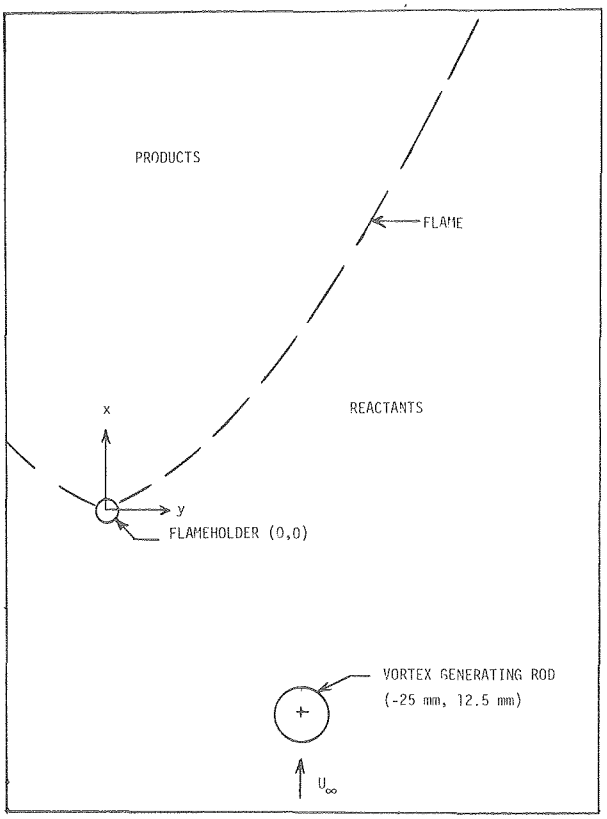

Fig. 1. Schematic diagram of flame holder, flame location, vortex generating rod, and undisturbed flow direction. (XBL 805-9543)

Flowfield surveys of velocity and density were made for three vortex shedding Reynolds numbers, Re_D, of 73, 110, and 500, Phase-locked flowfield surveys were made only for Re_D = 73 and 110. For reference, the frequency of vortex pair generation for the 2.0 mm rod, with a free stream flowfield of 55 m/s, was 30 Hz.

The mean and rms fluctuation of the x-component of the flow velocity is shown in Figure 2; two y-profiles taken at the same axial (x) location, but with 2.0 and 3.0 diameter vortex generating rods, are shown. Figure 3 shows a contour plot of the mean velocity (x component only). The flame front is identified as the region of sharp rise in velocity; the minimum upstream of the flame is caused by the wake of the vortex-generating rod. This minimum is deflected outward by the flame, as can be seen from the figure.

The phase-locked measurements are representative of the conditions at a certain time (phase

* This work was supported by the U.S. Air Force Office of Scientific Research under Contract No. F44620-76-C-0083 through the Campus Research Office of the University of California, Berkeley. Additional facility and equipment support was provided by the Director of the Office of Energy Research, Office of Basic Energy Sciences, Chemical Sciences Division of the U.S. Department of Energy under Contract No. W-7405-ENG-48.

† Present address: Department of Mechanical Engineering, Drexel University, Philadelphia, PA

†† Present address: Department of Mechanical Engineering, Columbia University, New York, NY

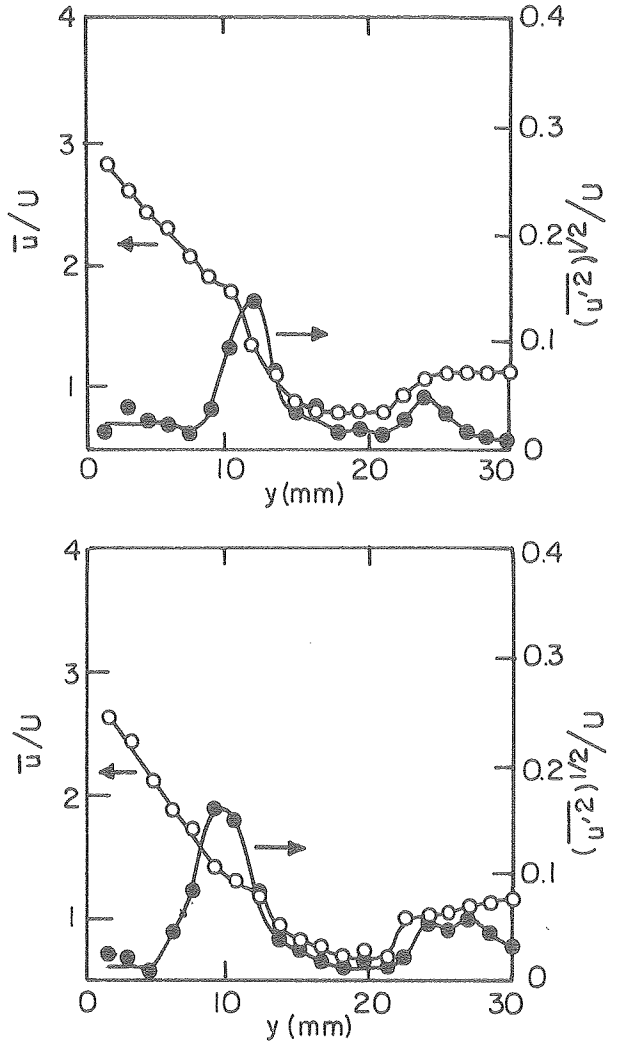

Fig. 2. Mean and rms fluctuation profiles of the x-component of the velocity, taken at a given axial location through the flame front and the vortex wake of the rod. The two figures are for (a) 2.0 mm and (b) 3.0 mm vortex generating rod. (XBL 808-5624)

angle) in the position of the vortex generated by the rod. The position of the vortex is obtained by a hot-wire sensor located in the wake region of the vortex-generating rod, upstream of the flame front. A constant velocity contour plot example at a given phase angle is shown in Figure 4, which can be considered to be an instantaneous "snapshot" of the velocity. Here, it is seen that the flame front is highly distorted by the wake. Further, vortices generated by the rod can be seen to be present upstream of the flame front but cannot be identified downstream of the flame in the burned gases. These measurements indicate that the turbulence level of the flow is drastically reduced by the flame, so much so that there do not appear to be identifiable vortex structures in the burned gas. This may be simply due to the combination of the flow dilatation and increased viscous dissipation in the burned gases. However, a more subtle interaction of the flame front with the vortex structure may serve to further reduce the overall vortex strength.

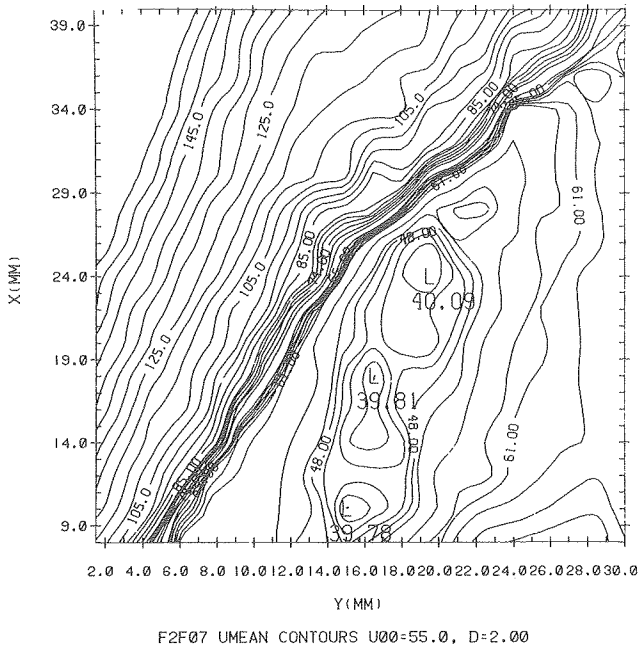

Fig. 3. Constant mean axial velocity contours for the flame in the wake of a 2.0 mm vortex generating rod. (XBL 812-8258)

One of the more interesting results of the density measurements is shown in Figure 5. This is a 3-D plot of the evolution of the probability density function of the gas density through the turbulent flame front. The horizontal axis is the ratio of the measured gas density to the unburned gas

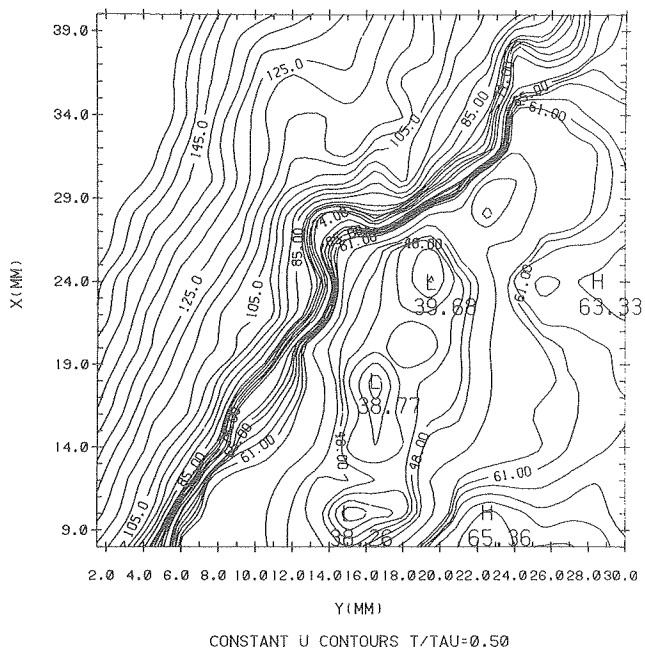

Fig. 4. Constant "instantaneous" axial velocity contours, at a given phase angle in the vortex generating cycle, for a flame in the wake of a 2.0 mm vortex generating rod. (XBL 812-8259)

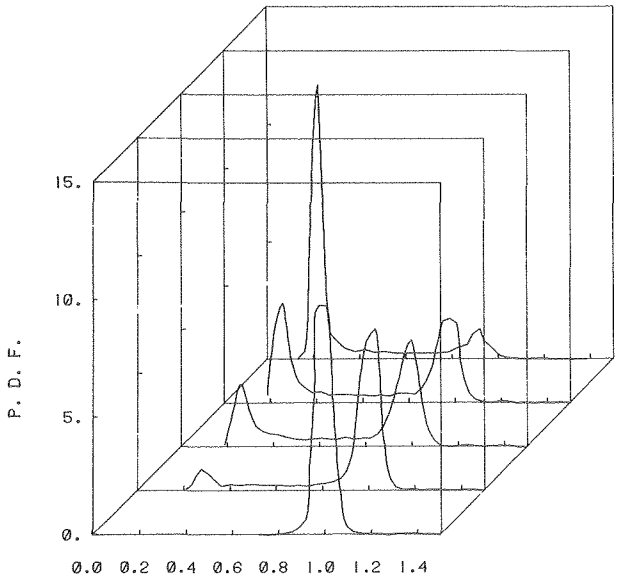

Fig. 5. Evolution of the probability density function (pdf) of the gas density as a function of position ($\tilde{c}$) through the fluctuating flame in the wake of a 2.0 mm vortex generating rod.

(XBL 808-11109)

density; the cold, unburned gas is located at 1.0 while the hot, burned gas is at 0.25. The position through the flame front is represented by $\tilde{c}$, a reaction progress variable. It can be seen that, at any point within the flame front, the gas tends to be either completely burned or unburned, with not much in between (a so-called bimodal distribution). Thus, the flame is fairly well represented by a thin fluctuating sheet, which can be highly contorted as indicated in Figure 4.

PLANNED ACTIVITIES FOR FY 1981

The experimental portion of this research has been completed and additional work is not presently planned. Numerical computations simulating a two-dimensional vortex interacting with a flame have been made[3] and further refinement of these computations is continuing. Further analysis of the experimental results is planned.

REFERENCES

1. I. Namer, "An Experimental Investigation of the Interaction between a Kármán Vortex Street and a Premixed Laminar Flame," University of California, College of Engineering Report FM-80-2, Ph.D. Thesis (1980).

2. I. Namer, Y. Agrawal, R. K. Cheng, F. Robben, R. Schefer, and L. Talbot, "Interaction of a Plane Flame Front with the Wake of a Cylinder," University of California, College of Engineering Report FM-77-3 (Oct. 1977).

3. I. Karasalo, A. J. Chorin, I. Namer, F. Robben, and L. Talbot, "Numerical Simulation of the Interaction of a Flame with a Kármán Vortex Street," Lawrence Berkeley Laboratory Report, LBL-10679 (1980).

MODELING OF BURNING AND EXTINCTION CHARACTERISTICS OF A POLYMER DIFFUSION FLAME AND COMPARISON WITH EXPERIMENT*

W. Pitz and R. Sawyer

INTRODUCTION

The importance and contribution of the inherrent flammability of polymeric materials to problems of fire safety is well recognized. This study was undertaken to provide a better understanding and interpretation of previous experimental investigations of polymer flammability. The structure of opposed flow diffusion flames have been measured by several investigators using both gaseous[1,2] and solid[3,4,5] fuels. The opposed flow diffusion flame is a convenient geometry for the study of the flammability of polymers because it allows both steady, diffusion controlled burning and extinction to be observed under well-controlled laboratory conditions. Conveniently available experimental parameters include fuel composition, oxidizer composition, and oxidizer blowing rate. Reported experiments generally have not included the variation of pressure or temperature. Radiation effects, which are important in fires, remain to be well-characterized in laboratory studies of opposed flow diffusion flames where radiation generally is of minor importance.

ACCOMPLISHMENTS DURING FY 1980

Reacting flow in a stagnation point boundary layer was modelled with the objective of examining its properties near extinction, Figure 1. Axisymmetric geometry, laminar-flow, and steady-state combustion were considered to conform to an existing diffusion flame burner[5]. Variation of fluid properties with both temperature and composition was included. The specific heats of the three species considered (fuel, oxygen and products) were chosen to be those of ethylene, oxygen, and nitrogen respectively, and approximated as cubic functions of temperature. The effective viscosity was obtained from the individual, temperature-dependent viscosities using Wilke's mixture rule[6]. The Prandtl number was fixed at 0.7, which is a good approximation for the reactants and products considered. The Lewis number was assumed to be 1.

Finite reaction rate chemistry was incorporated with a one-step reaction and Arrhenius rate expression. Three species were considered: fuel, oxygen and products. The reaction rate was of order one with respect to both fuel and oxygen.

The boundary conditions for the N_2/O_2 flow were an ambient temperature of 294K and a pressure

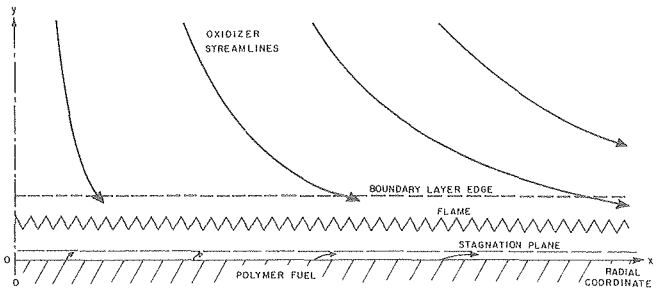

Fig. 1. Description of a reacting, stagnation-point flow. (XBL 811-5106)

of 1 atm. The polymer burning rate was calculated from the enthalpy gradient at the fuel surface and the effective latent heat. The latent heat was extracted from the mass transfer B number, previously reported by Holve and Sawyer,[7] based on their experimental observation of the combustion poly (ethylene) in an opposed flow diffusion flame, $B = 3.48Y_{O}^{\infty}-0.18$, where Y_{O}^{∞} is the oxygen mass fraction in the ambient N_2/O_2 flow. The fuel surface temperature was specified at 800K. The oxygen concentration at the fuel surface was set at zero. The fuel surface mass fraction, Y_{fw}, results from species and energy balances,

$$Y_{fw} = (B - Y_{O}^{\infty}/s)/(1 + B) \qquad (1)$$

where s is the stoichiometric ratio, mass fuel consumed per mass of oxygen.

Solutions to the boundary layer equations were found by using GENMIX,[8] which solves the finite difference equations in implicit form. The flame structure was found for both finite and infinite reaction rate cases for an oxygen mole fraction, X_{O}^{∞}, of 0.232 as shown in Figures 2 and 3. If only a solid curve appears on the profiles, the finite and infinite reaction-rate curves are super-imposed for this graph size. For an infinite reaction rate, the oxygen and fuel concentrations go to zero at the maximum temperature location, which will be designated the flame. When the reaction rate is finite, some of the fuel and oxygen survive and are transferred through the flame. Transfer of molecular oxygen through the flame was also found experimentally, as shown by the experimental points in Figure 2.

The velocity profiles for the finite and infinite reaction rate are identical on the graphic scale presented. The variable u/u_{max} is plotted because it is independent of radial location. The

* This work was supported through the U.S. National Bureau of Standards under Contract No. 805180 through the U.S. Department of Energy under Contract No. W-7405-ENG-48 .

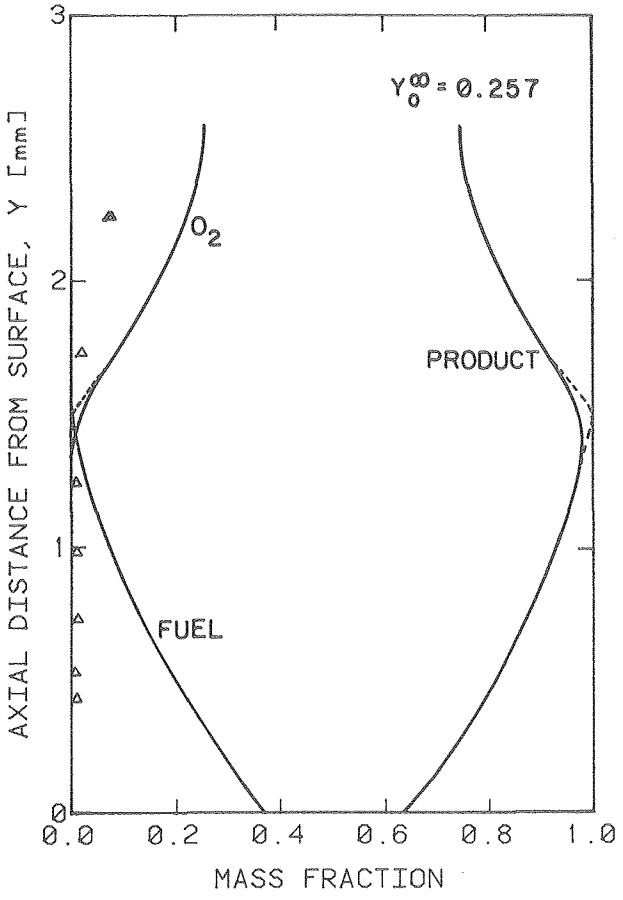

Fig. 2. Calculated species profiles for finite (——) and infinite (---) reaction rates. Measured oxygen profile (Δ). (XBL 811-5110)

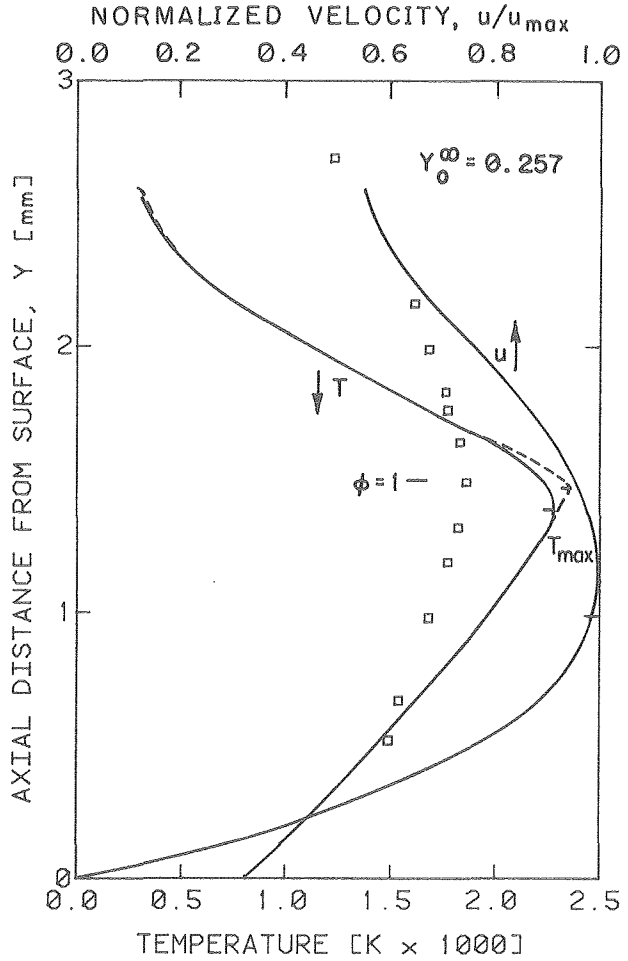

Fig. 3. Calculated temperature profiles for finite (——) and infinite (---) reaction rates. Measured temperature profile (□). Calculated velocity profile. (XBL 811-5109)

location of u_{max} is between the flame and fuel surface for the following reasons. Since the viscosity is temperature dependent, it is maximum at the flame. As indicated in Figure 1, the streamlines pass through the flame convecting the flow into this lower viscosity region where the maximum velocity is attained.

Calculated flame stand-off distances for finite and infinite reaction rates and measured stand-off distances are shown in Figure 4. All stand-off distances presented decrease with decreasing ambient oxygen mole fraction, X_O^∞. When X_O^∞ is lowered, the flame temperature is reduced, which decreases temperature gradient at the surface and, thereby, the fuel blowing rate. The fuel mass fraction at the surface is also decreased since the B number is lowered (eq. 1). Both of these effects reduce the flame stand-off distance. It is crucial to include finite rate flame chemistry when predicting flame stand-off distances near extinction (Fig. 4). When X_O^∞ is increased, the flame condition moves out of the extinction regime, and the flame stand-off distance predictions are the same for both finite and infinite rate cases. If the flame is near extinction, the net fluid motion through the flame and towards the surface becomes important. The reactants are convected for significant distance before they are fully reacted and the maximum temperature is reached.

Overall reaction-rate parameters were extracted from extinction data. Extinction measurements in the opposed flow apparatus were performed for poly(ethylene) burning in N_2/O_2 mixtures (Fig. 5). The values of the reaction-rate parameters were iterated until the calculated extinction curve approximated the least squares fit of the data. The resultant activation energy, E_A, and pre-exponential coefficient, K, are defined by the following Arrhenius expression,

$$\dot{m}_f = K\, p^2\, Y_f\, Y_O\, \exp(-E_A/RT)$$

where E_A is 31 ± 3 kcal/gmole, K is 5.4×10^{-2} kg/(Pa)^{2}m^{3}s, $\dot{m}_f$ is the mass consumption rate of fuel per unit volume in kg/Pa^{2}m^{3}s, p is the pressure in Pa, Y_f and Y_O are the fuel and oxygen mass fractions, R is the gas constant, and T is the temperature in K.

PLANNED ACTIVITIES FOR FY 1981

Measurements of inhibition characteristics and the final report of this study will be accomplished and this research will then be concluded.

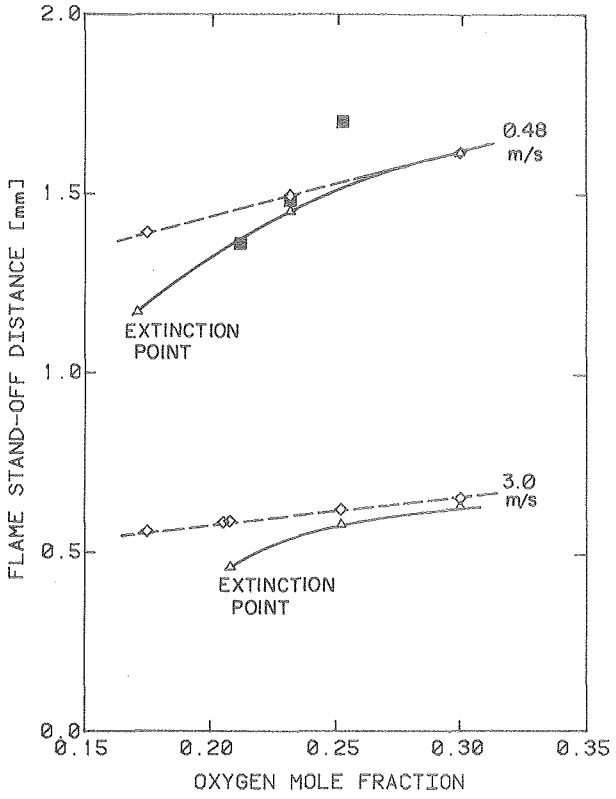

Fig. 4. Flame stand-off distance calculated for finite (——) and infinite (---) reaction-rate and measured by experiment (□). (XBL 811-5111)

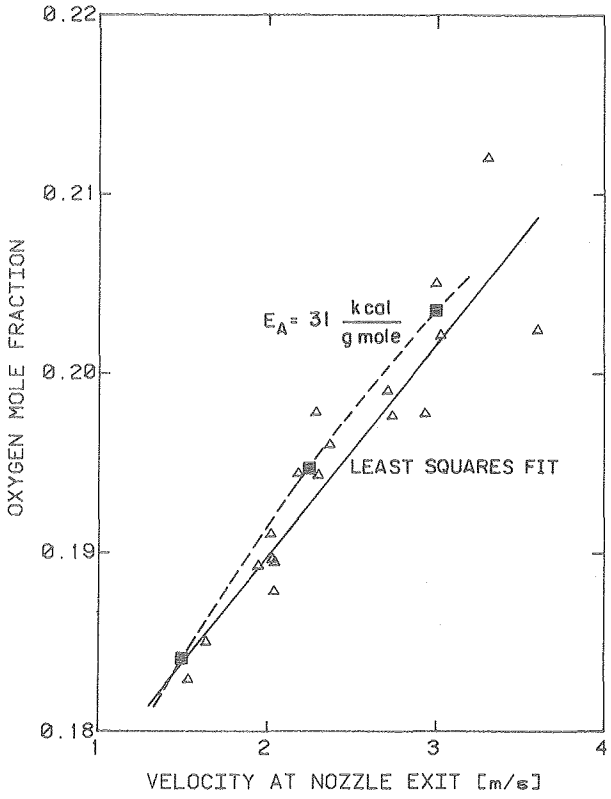

Fig. 5. Measured extinction conditions for PE burning in N_2/O_2 mixtures (△) and calculated extinction conditions (□). (XBL 811-5113)

REFERENCES

1. T. P. Pandya and F. J. Weinberg: Proc. Roy Soc. A., vol. 279, p. 544 (1965).

2. H. Tsuji and I. Yamaoka: Twelfth Symposium (International) on Combustion, The Combustion Institute, p. 997 (1969).

3. J. R. Richard, C. Vovelle, and R. Delbourgo: Fifteenth Symposium (International) on Combustion, The Combustion Institute, p. 205 (1975).

4. K. Seshadri and F. A. Williams: J. Polymer Sci.: Polymer Che. Ed., vol. 16, p. 1755 (1978).

5. W. J. Pitz, N. J. Brown and R. F. Sawyer: Eighteenth Symposium (International) on Combustion, The Combustion Institute, 1981.

6. C. R. Wilke: J. Chem. Phys., vol. 18, p. 517 (1950).

7. D. J. Holve and R. F. Sawyer: Fifteenth Symposium (International) on Combustion, The Combustion Institute, p. 351 (1975).

8. D. B. Spalding: GENMIX: A General Computer Program for Two-Dimensional Parabolic Phenomena, Pergamon Press (1977).

FLAME RADIATION*

C. Tien and S. Lee

INTRODUCTION

Thermal radiation from flames has long been recognized as an important factor in many physical systems, such as fires and combustors. The combustion products from flames of hydrocarbon fuels generally consist of several gas constituents plus numerous unburnt solid particulates called soot. Soot particles in flames contribute significantly to the infrared radiation, as well as the luminosity of flames. To estimate the radiative contribution of soot to flames, detailed soot information must be known.

Soot particles are characterized by optical properties, composition (hydrogen/carbon ratio), size distributions, and shapes. By assuming the soot is spherical, other properties, as well as radiative heat transfer analyses, have been explored in several previous investigations.[1-5]

In the past, research progress was concerned primarily with the physical and specific analytical basis of infrared radiation from flames. The fundamental aspects of soot characteristics, such as soot optical properties, composition, shapes, and measurements of soot volume fraction for various flames, were determined.

ACCOMPLISHMENTS DURING FY 1980

Research during the past year was focused on obtaining the various characteristics of soot and determining their effect on soot radiation and heat transfer. These are discussed below.

Soot Optical Properties and the Effect of Composition

A dispersion model has been established for the optical constants of soot in hydrocarbon flames on the basis of a more rigorous consideration of the electronic band structure and the dispersion constants.[6] The dispersion constants of hydrocarbon soot have been determined from this model in conjunction with the in-situ flame transmission data in the visible and infrared ranges, thus truly reflecting soot in flames. It is shown that the soot optical properties are rather insensitive to temperature changes at elevated temperatures, but the room temperature values representative of soot in smoke do exhibit appreciable deviation.

On the experimental side, transmission experiments were performed to obtain the spectral extinction coefficients and volume fractions of soot from various flames. Agreement between the experimental and predicted results is excellent. The results also indicate that the soot optical properties are relatively independent of the fuel hydrogen/carbon ratio.

Soot Particle Shape

The radiative heat transfer characteristics of a sooty medium may vary greatly because of soot conglomeration. Information on the number of various conglomerated shapes is required for the exact calculation of flame and smoke radiation. The complexities and uncertainties involved in accounting for all particle shapes present a formidable problem and may not justify any detailed or elaborate computation for practical applications. Therefore, radiation from different particle shapes was investigated recently[7] to develop a better understanding of the effect of soot conglomeration on soot radiation.

Radiative Heat Transfer with Particulate Scattering

The resistance-network representation for radiative heat transfer is developed for a planar absorbing-scattering medium on the basis of the two-flux model and the linear anisotropic scattering model.[8] Particular attention is given to the scattering effect caused by particulates such as flame soot or smoke particles. Limiting relations for various regimes are derived and the physical significance of the resistances are discussed. An illustrative example is presented for thermal radiation from a smoke layer. Extension to two-phase dispersed systems is also demonstrated.

REFERENCES

1. R. O. Buckius and C. L. Tien, "Infrared Flame Radiation," International Journal of Heat and Mass Transfer, vol. 20, pp. 93-106 (1977).

2. W. W. Yuen and C. L. Tien, "A Simple Calculation Scheme for the Luminous-Flame Emissivity," Proceedings of the 16th International Combustion Symposium, pp. 1481-1487 (1977).

3. G. L. Hubbard and C. L. Tien, "Infrared Mean Absorption Coefficients for Luminous Flames and Smoke," Journal of Heat Transfer, vol. 100, pp. 235-239 (1978).

4. W. W. Yuen and C. L. Tien, "Approximate Solutions of Radiative Transfer in One-Dimensional Non-Planar Systems," Journal of Quantitative Spectroscopy and Radiative Transfer, vol. 19, pp. 533-549 (1978).

5. W. W. Yuen and C. L. Tien, "A Successive Approximation Approach to Problems in Radiative Transfer with a Differential Formulation," Journal of Heat Transfer, vol. 102 (1980).

* This work was supported by the Center for Fire Research of the U.S. National Bureau of Standards under Contract No. NB80NAGE1653 through the U.S. Department of Energy under Contract No. W-7405-ENG-48.

6. S. C. Lee and C. L. Tien, "Optical Constants of Soot in Hydrocarbon Flames," Proceedings of the 18th International Combustion Symposium (1980).

7. S. C. Lee and C. L. Tien, "Thermal Radiation of Spherical and Cylindrical Soot Particles," Paper presented at the Western States Section/ The Combustion Institute, Paper No. 80-54, Fall Meeting, Los Angeles, CA., October 20-21, 1980.

8. T. W. Tong and C. L. Tien, "Network Representation of Radiative Heat Transfer with Particulate Scattering," Journal of Quantitative Spectroscopy and Radiative Transfer, vol. 24, pp. 491-503 (1980).

TESTS AND CRITERIA FOR FIRE PROTECTION OF CABLE PENETRATIONS*

R. Williamson and F. Fisher

INTRODUCTION

The spread of fire in nuclear reactors depends critically on the barrier qualities of the cable penetrations of fire resistant walls and floor/ceiling assemblies. The ASTM E-119 Fire Endurance Test Method has been used to qualify the unpenetrated walls and floor/ceiling assemblies; but, if such assemblies contain cable penetrations, special attention is required. This is the focus of this project.

The actual fire conditions represented by the E-119 test method, termed "post-flashover," are conditions in which fire fully involves a compartment. Post-flashover fires are characterized by a positive pressure differential between the upper half of the fire compartment and the unexposed face of the wall and floor/ceiling assemblies which make up its boundaries. The initial portion of this post-flashover period is also characterized by excess amounts of fuel which have been pyrolized by the fire within the compartment. The positive pressure and excess pyrolyzate are clearly proven by the flames which commonly are observed to emerge from the doors and windows of both actual and laboratory post-flashover building fires.

The ASTM E-119 Standard does not specify either the pressure differential or the presence of excess fuel at the surface of the test assembly. One of the objectives of this project has been to establish the effects of varying furnace pressure on cable penetrations performance in the ASTM E-119 fire test. Another objective has been to investigate the modes of failure for these cable penetrations and to explore the possibility of new pass/fail criteria.

Experiments were conducted during 1979 which clearly showed that positive pressure and excess pyrolyzates play a vital role in the spread of fire through cable penetrations. If there is a path through the penetration opening, flames always appear on the unexposed face when there is a positive pressure differential and there are excess pyrolyzates in the furnace.

ACCOMPLISHMENTS DURING FY 1980

A draft fire test proposal for positive pressure and excess pyrolyzates was written and circulated to the appropriate Task Group and Subcommittee in the American Society for Testing and Materials where both fire protection and nuclear engineers participated. There has been an extensive debate on these measures, and it now appears (as of January 1981) that the non-nuclear interests on the ASTM committee have dominated the issue and that the penetration test standard will not call for either positive pressure or excess pyrolyzates, although the former will be an option.

Experimental fire tests were conducted during 1980 to establish the best methods of regulating pressure and providing excess pyrolyzates during the ASTM E-119 test.[1] It was found that the pressure was relatively easy to regulate using dampers on the furnace stacks, but the excess pyrolyzates were much more difficult to control. Part of the problem is that, with both positive pressure and excess pyrolyzates, the Standard E-119 time-temperature curve is very difficult to maintain. In some experiments, we had a runaway fire with a much greater "severity" than the relatively benign E-119 fire.

The net results of the circulation of draft fire test standards through the ASTM, in conjunction with the experimental difficulties, has lead to the realization that it is not sufficient to add additional requirements to the ASTM E-119 Test Method in order to evaluate cable penetrations; it will be much better to develop an entirely new fire test standard.

Another accomplishment during 1980 has been the development of a probabilistic network for fire spread. A paper entitled "Using Fire Tests for Quantitative Risk Analysis" was presented at the ASTM Symposium on "Risk Analysis" at Hilton Head, S.C., June, 1980, describing the use of fire tests.

* This work was supported by the U.S. Nuclear Regulatory Commission through Sandia Laboratories, Albuquerque, New Mexico under Contract No. 46-6967 through the U.S. Department of Energy under Contract No. W-7405-ENG-48.

In the course of preparing this paper, a new and potentially revolutionary approach to fire protection was discovered. This is the subject of a proposal for new research as follows:

"Quantitative Fire Risk Analysis
Utilizing Probabilistic Methods"

The application of networks to solve fire protection problems has led to a new method of quantitative analysis. If the networks for fire spread, smoke development, and evacuation of occupants are converted to probabilistic networks, such as those used in communications engineering, these networks can be solved simultaneously to quantify a range of fires which could occur in a given building. The possible fires, their expected potential for injury to occupants, and their potential for property damage would be explicitly presented. The research project has two principal objectives: first, the development of probabilistic networks for fire and smoke spread and the movement of people, and emphasis in designing these for simultaneous solution; second, there would be an experimental program to develop the methods of gathering the physical data to quantify the probabilistic networks.

This proposed research project is oriented toward the environmental health and safety of buildings. The recent tragic fire in the MGM Grand Hotel in Las Vegas, where 84 persons died, shows the continuing problem of unwanted fire. This research project is focused on a new and powerful method of analyzing the fire safety of buildings. It has potential application in many areas of special interest to DOE, such as conservation, solar power, and nuclear power. The use of new materials and new building designs requires a careful analysis for fire safety before a disastrous fire emphasizes the problem. Support of this new research will be sought from various potential sponsors.

PLANNED ACTIVITIES FOR FY 1981

A special floor fire-test furnace, constructed for another project, will be used to perform experiments on cable penetration assemblies, with specific pressure and excess pyrolyzates on the fire side of the test specimen. The emphasis in the research will be to investigate the experimental methods required to subject cable penetrations to the range of potential fires which they might face under actual fire conditions.

REFERENCE

1. Annual Book of ASTM Standards, American Society for Testing and Materials, Philadelphia, PA.